

15. Gottumukkala V, Luguya R, Fronczek FR, Vicente MG. Synthesis and cellular studies of an octa-anionic 5,10,15,20-tetra[3,5-(nido-carboranyl)methyl]phenyl]porphyrin (H(2)OCP) for application in BNCT. *Bioorg Med Chem* 2005; 13(5):1633–1640.
16. Friso E, Roncucci G, Dei D, Soncin M, Fabris C, Chiti G, Colautti P, Esposito J, De Nardo L, Riccardo Rossi C, Nitti D, Giuntini F, Borsetto L, Jori G. A novel ¹⁰B-enriched carboranyl-containing phthalocyanine as a radio- and photo-sensitizing agent for boron neutron capture therapy and photodynamic therapy of tumours: In vitro and in vivo studies. *Photochem Photobiol Sci* 2006;5(1):39–50.
17. Coderre JA, Button TM, Mica PL, Fisher CD, Nawrocky MM, Liu HB. Neutron capture therapy of the 9L rat gliosarcoma using the p-boronophenylalanine-fructose complex. *Int J Radiat Oncol Biol Phys* 1994;30(3):643–652.
18. Barth RF. Rat brain tumor models in experimental neuro-oncology: The 9L, C6, T9, RG2 (D74), RT-2 and CNS-1 gliomas. *J Neurooncol* 1998;36(1):91–120.
19. Biston MC, Joubert A, Adam JF, Elleaume H, Bohic S, Charvet AM, Estève F, Foray N, Balosso J. Cure of Fisher rats bearing radioresistant F98 glioma treated with cis-platinum and irradiated with monochromatic synchrotron X-rays. *Cancer Res* 2004;64(7):2317–2323.
20. Kobayashi N, Allen N, Clendenon NR, Ko LW. An improved rat brain-tumor model. *J Neurosurg* 1980;53(6):808–815.
21. Taylor HJ, Goldhaber M. Detection of nuclear disintegration in a photographic emulsion. *Nature* 1935;135:341–341.
22. Snyder HR, Reedy AJ, Lennarz WJ. Synthesis of aromatic boronic acids. Aldehyde boronic acids and a boronic acid analog of tyrosine. *J Am Chem Soc* 1958;80:835–838.
23. Soloway AH, Hatanaka H, Davis MA. Penetration of brain and brain tumor: VII. Tumor-binding sulfhydryl boron compounds. *J Med Chem* 1967;10(4):714–717.
24. Dougherty TJ, Gomer CJ, Henderson BW, Jori G, Kessel D, Korbelik M, Moan J, Peng Q. Photodynamic therapy. *J Natl Cancer Inst* 1998;90(12):889–905.
25. Stummer W, Novotny A, Stepp H, Goetz C, Bise K, Reulen HJ. Fluorescence-guided resection of glioblastoma multiforme by using 5-aminolevulinic acid-induced porphyrins: A prospective study in 52 consecutive patients. *J Neurosurg* 2000;93(6):1003–1013.
26. Fairchild RG, Saraf SK, Kalef-Ezra J, Laster BH. Comparison of measured parameters from a 24-keV and a broad spectrum epithermal neutron beam for neutron capture therapy: An identification of consequential parameters. *Med Phys* 1990; 17(6):1045–1052.

Computed Tomography Imaging of Transferrin Targeting Liposomes Encapsulating Both Boron and Iodine Contrast Agents by Convection-Enhanced Delivery to F98 Rat Glioma for Boron Neutron Capture Therapy

Shiro Miyata, MD*
 Shinji Kawabata, MD, PhD*
 Ryo Hiramatsu, MD*
 Atsushi Doi, MD, PhD*
 Naokado Ikeda, MD, PhD*
 Taro Yamashita, MD*
 Toshihiko Kuroiwa, MD, PhD*
 Satoshi Kasaoka, PhD‡
 Kazuo Maruyama, PhD§
 Shin-ichi Miyatake, MD, PhD*

*Department of Neurosurgery, Osaka Medical College, Osaka, Japan; †Faculty of Pharmaceutical Sciences, Hiroshima International University, Hiroshima, Japan; ‡Faculty of Pharmaceutical Sciences, Teikyo University, Tokyo, Japan.

Correspondence:

Shinji Kawabata, MD, PhD,
 Department of Neurosurgery,
 Osaka Medical College,
 2-7 Daigaku-machi,
 Takatsuki City,
 Osaka 569-8686, Japan.
 E-mail: neu046@poh.osaka-med.ac.jp.

Received, February 4, 2010.

Accepted, October 2, 2010.

Copyright © 2011 by the
 Congress of Neurological Surgeons



WHAT IS THIS BOX?

A QR Code is a matrix barcode readable by QR scanners, mobile phones with cameras, and smartphones. The QR Code above links to Supplemental Digital Content from this article.

BACKGROUND: To achieve potent tumor-selective antitumor efficacy by boron neutron capture therapy (BNCT), it is important to have a significant differential uptake of ^{10}B between tumor cells and normal cells. This should enable BNCT to reduce damage to normal tissues compared with other radiation therapies.

OBJECTIVE: To augment the therapeutic efficacy of BNCT, we used transferrin-conjugated polyethylene glycol (PEG) (TF-PEG) liposome encapsulating sodium borocaptate and iomeprol, an iodine contrast agent, with intratumoral convection-enhanced delivery (CED) in a rat glioma tumor model.

METHODS: The in vitro ^{10}B concentration of F98 rat glioma cells was determined by inductively coupled plasma atomic emission spectrometry after incubation with either TF-PEG or PEG liposomes. For in vivo biodistribution studies, ^{10}B concentrations within blood, normal brain tissue, and intracerebrally transplanted F98 cells were measured with inductively coupled plasma-atomic emission spectrometry after CED of the compounds, and computed tomography was performed at selected time intervals.

RESULTS: ^{10}B concentrations of F98 cultured glioma cells in vitro 6 hours after exposure to PEG and TF-PEG liposome were 16.1 and 51.9 ng $^{10}\text{B}/10^6$ cells, respectively. ^{10}B concentrations in F98 glioma tissue 24 hours after CED were 22.5 and 82.2 $\mu\text{g}/\text{g}$, by PEG and TF-PEG liposome, respectively, with lower ^{10}B concentrations in blood and normal brain. Iomeprol provided vivid and stable enhanced computed tomography imaging of the transplanted tumor even 72 hours after CED by TF-PEG liposome. Conversely, tissue enhancement had already washed out at 24 hours after CED of the PEG liposomes.

CONCLUSION: The combination of TF-PEG liposome encapsulating sodium borocaptate and iomeprol and intratumoral CED enables not only a precise and potent targeting of boron delivery to the tumor tissue, but also the ability to follow the trace of boron delivery administered intratumorally by real-time computed tomography.

KEY WORDS: Boron neutron capture therapy, Computed tomography, Convection-enhanced delivery, Liposome, Transferrin

Neurosurgery 68:1380–1387, 2011

DOI: 10.1227/NEU.0b013e31820b52aa

www.neurosurgery-online.com

ABBREVIATIONS: ^{10}B , boron-10; **BBB**, blood-brain barrier; **BDS**, boron delivery system; **BNCT**, boron neutron capture therapy; **BSH**, sodium borocaptate; **CED**, convection-enhanced delivery; **PEG**, polyethylene glycol; **TF-PEG**, transferrin-conjugated polyethylene glycol

Supplemental digital content is available for this article. Direct URL citations appear in the printed text and are provided in the HTML and PDF versions of this article on the journal's Web site (www.neurosurgery-online.com).

Therapeutic modalities such as stereotactic radiosurgery, intensity-modulated radiation therapy, particle radiation therapy, and novel therapeutic agents with molecular targeting have been developed to improve the prognosis of some types of brain tumors. However, over the past few decades, there has been little improvement in the prognosis of

patients with malignant gliomas because of the tumor's tendency to microscopically infiltrate the surrounding normal tissue. To overcome this infiltrative nature, it is necessary to selectively deliver a higher concentration of anticancer or radiation sensitizing agents into tumor tissue compared with the surrounding normal brain tissue. We are focusing on developing boron neutron capture therapy (BNCT) to achieve greater tumor-selective killing and therefore therapeutic efficacy.

At our institution, we have clinically applied BNCT since 2002 as an essential adjuvant therapy for patients with recurrent or newly diagnosed malignant gliomas¹⁻⁴ and have achieved superior outcomes compared with those by standard therapies using fractionated radiographic treatments.⁵ BNCT is based on the nuclear capture and fission reactions that occur when boron-10 (¹⁰B), a nonradioactive constituent of natural elemental boron, is irradiated with low-energy thermal neutrons to produce high-energy α particles and recoiling lithium-7 nuclei. These have high linear energy transfer and path lengths of approximately 9 and 5 μ m, respectively, which theoretically allow them to discharge their energy within ¹⁰B-containing cells.⁶ Thus, to achieve potent tumor-selective antitumor efficacy, it is important to have a significant differential uptake of ¹⁰B between tumor cells and normal cells. This should enable BNCT to reduce damage to normal tissues compared with other radiation therapies.

Today, clinically used sodium borocaptate (BSH) is transferred to brain tumors only through the disrupted blood-brain barrier (BBB), so it is difficult for BSH to reach regions that tumor cells invade microscopically where the BBB seems to be intact. On the other hand, boronophenylalanine, which transfers boron via L-type amino acid transporter, can deliver ¹⁰B even in the infiltrating tumor cell population where the BBB is intact. However, some amounts of ¹⁰B are inevitably taken into the normal cells by boronophenylalanine systemic administration. Moreover, the native heterogeneity of malignant gliomas interferes with the ability to accurately target the tumor. Recent reports have delineated boron delivery systems (BDSs) to improve molecular targeting of malignant gliomas.^{7,8} Previously we reported on the effectiveness of transferrin-conjugated polyethylene glycol (PEG) (TF-PEG) liposome encapsulating BSH administered intravenously, with regard to its ability to target tumor cells and to increase the accumulation of ¹⁰B in tumor tissue.⁹

To improve the efficacy of tumor targeting under systemic administration, the circulation time of a BDS in the blood needs to be lengthened. Unfortunately, systemic administration of a BDS increases the capture of ¹⁰B-labeled molecules in the reticuloendothelial system of the liver and spleen, which may cause adverse effects. To solve these problems, we adopted convection-enhanced delivery (CED) for drug administration. This technique enables the delivery of boron compounds to the tumor cells in the brain without going through the disrupted BBB. CED, a method for local drug infusion directly into the brain,¹⁰ enables the distribution of any drugs homogeneously in the brain, keeping high concentration at the target site without mechanical damage to the surrounding normal tissue. CED depends on the bulk flow in the

interstitial space produced by continuous slow infusion into the brain under low positive pressure. Using this method, it is theoretically possible to deliver drugs to regions where tumor cells invade microscopically with little accumulation in the blood and other organs. Moreover, because it does not depend on the molecular weight of the infused agent, this method allows us to widely select many kinds of therapeutic agents or carriers for them, such as liposomes, dendrimers, and nanotubes.^{7,11-15} Today, some clinical trials of targeted toxins with epidermal growth factor receptor, transferrin receptor, interleukin-13 receptor, and interleukin-4 receptor are reported.^{8,11,16-18}

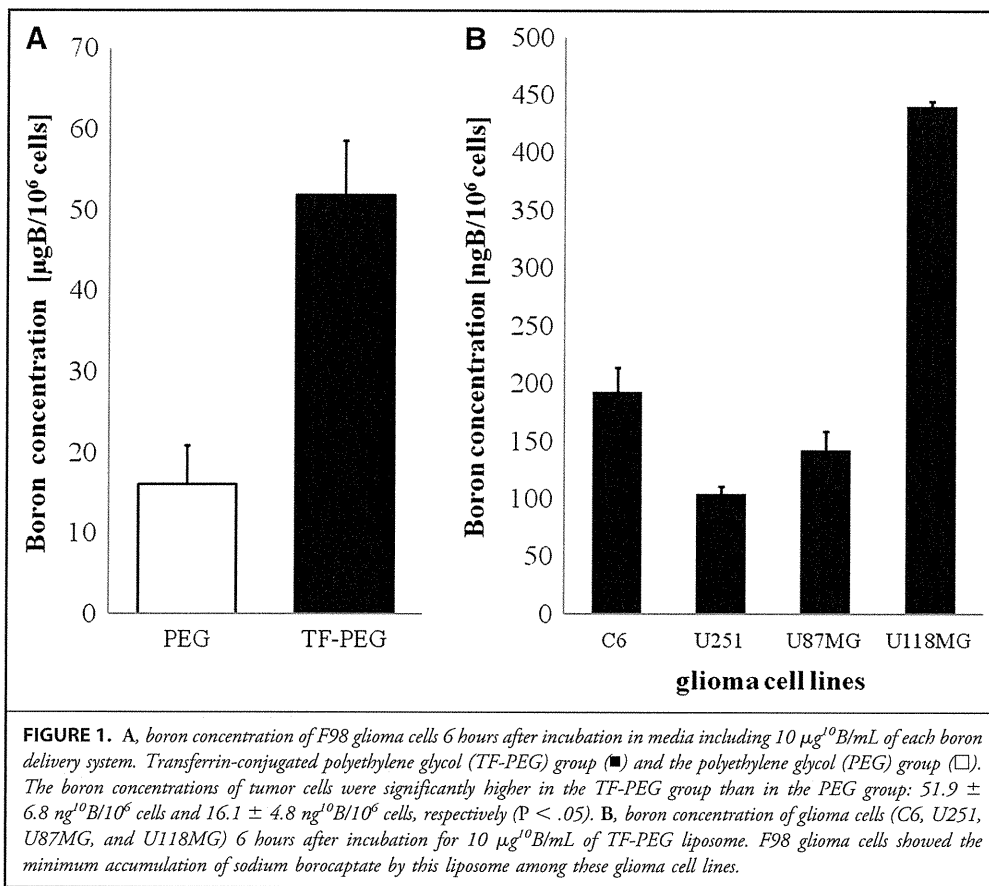
In BNCT, there is some interval before neutron irradiation, unlike with chemotherapies or therapies by toxins. This interval derives from the nontoxicity of BDS, and it enables us to estimate the distribution of infusion agents before neutron irradiation. We developed a novel liposomal BDS mechanism that encapsulates BSH and an iodine contrast agent, making it possible to trace the intracerebral distribution of the drug by computed tomography (CT).¹⁹ We evaluated 2 BDSs: PEG liposome encapsulating both BSH and Iomeprol (PEG liposome [BSH, Iomeprol]) and TF-PEG liposome (BSH, Iomeprol) administered by CED in rat brain tumor models.

MATERIALS AND METHODS

Preparation of the Boron Compounds

BSH was purchased from Katchem (Prague, Czech Republic). Iomeprol was used as an iodine contrast agent for CT scanning. Iomeprol (MW777.09, concentration 612.4 mg/mL; Iomeron 300; Eisai, Tokyo, Japan), which is very soluble in water and contains 300 mg/mL organically bound iodine, was used as the imaging tracer. PEG liposome (BSH, Iomeprol) and TF-PEG liposome (BSH, Iomeprol) were prepared by one of the authors (S.K.) as reported previously.²⁰ Transferrin (1:60 transferrin:phospholipid molar ratio; phospholipid concentration, 0.2 mM) (Wako Pure Chemical Industries, Osaka, Japan) was conjugated to the distal ends of 1,2-dioleoyl-sn-glycero-3-phosphoethanolamine-n-[poly(ethyleneglycol)]-hydroxy succinamide (Nippon Oil and Fats, Tokyo, Japan) in micelles at room temperature for 1 hour with gentle stirring. TF-PEG distearoylphosphatidylethanolamine (DSPE) was transferred to preformed PEG liposomes (64:33:3 dipalmitoylphosphatidylcholine (DPPC):cholesterol:DSPE-PEG molar ratio; size <150 nm) loaded with 300 mM BSH:Iomeprol at a 1:1 volume ratio using the micelle transfer method at a 1:33 TF-PEG-DSPE:liposome molar ratio, at 45°C for 3 hours. Both PEG liposome (BSH, Iomeprol) and TF-PEG liposome (BSH, Iomeprol) were prepared using the protocol described by Wei et al⁷ with slight modifications.

To evaluate possible adverse effects of PEG liposome (BSH, Iomeprol) and TF-PEG liposome (BSH, Iomeprol) on normal brain parenchyma, 12 Fischer 344 male rats (200-230 g, F344 NSL; Japan SLC, Shizuoka, Japan) were given a 20- μ g ¹⁰B infusion of either BDS (n = 6 per BDS) into the right hemisphere by CED. Body weight was measured just before the CED procedure and on days 7 and 14 after the procedure. Some of the rats that were administered either BDS were euthanized on day 7 after the CED procedure for histological evaluation and were perfused with 4% paraformaldehyde; their brains were then processed for histological examination with hematoxylin and eosin staining.



In Vitro Cellular Uptake Study

For the in vitro boron uptake study, F98 rat glioma cells (provided by Rolf F. Barth MD, The Ohio State University, Columbus, Ohio) were used. One million F98 glioma cells were seeded onto a tissue culture dish (100 × 20 mm; Becton Dickinson, Franklin Lakes, New Jersey) with Dulbecco modified Eagle medium with 10% fetal bovine serum with penicillin and streptomycin at 37°C in an atmosphere of 5% CO₂. All the materials for the culture medium were purchased from Invitrogen (Carlsbad, California). After incubation for 24 hours at 37°C, the medium was replaced with Dulbecco modified Eagle medium containing 10 $\mu\text{g}^{10}\text{B}/\text{mL}$ PEG liposome (BSH, Iomeprol) or TF-PEG liposome (BSH, Iomeprol), and the cells were incubated for an additional 6 hours at 37°C. The medium was then removed, and the cells were washed twice with phosphate-buffered saline and detached with trypsin–ethylenediamine tetraacetic acid solution. Medium was then added, and the cells were counted and sedimented. Cells were digested overnight with 1 N nitric acid solution (Wako Pure Chemical Industries), and boron uptake was determined by inductively coupled plasma-atomic emission spectrometry (Hitachi, Tokyo, Japan). Cellular uptake of boron by TF-PEG liposome (BSH, Iomeprol) for other glioma cell lines (C6, U251, U87MG, and U118MG) was also evaluated.

Tumor Model

The male Fischer 344 rats were generally anesthetized with an intraperitoneal injection of pentobarbital sodium (50 mg/kg) and placed in

a stereotactic frame (Model 900; David Kopf Instruments, Tujunga, California). A midline incision was made in the scalp, and the skull target (3.5 mm right to the bregma) was identified. A hand-held drill was used to create a small burr hole at this location. A 25 μL Hamilton infusion syringe (model 1700 RN, Hamilton Bonaduz AG, Bonaduz, Switzerland) was fixed on the clamping device of the stereotactic frame. A 26-gauge needle attached to a microsyringe was first inserted to a depth of 6.0 mm from the skull and then withdrawn to its target depth in the brain (5.5 mm from the skull surface). Ten thousand F98 cells diluted in 10 μL of Dulbecco modified Eagle medium were then injected over approximately 10 minutes. The needle was kept in place for 1 minute after infusion and withdrawn slowly. The skull hole was sealed with bone wax, and the scalp was sutured. Under these conditions, the procedure results in tumor growth in all rats, with a median survival time of 23 days.

In Vivo Biodistribution Study

For biodistribution study, 10 days after tumor implantation, rats bearing F98 brain tumors were generally anesthetized and placed in a stereotactic frame as described above. They were administered either PEG liposome (BSH, Iomeprol) or TF-PEG liposome (BSH, Iomeprol) by CED with an infusion syringe pump over 30 minutes at a rate of 0.33 $\mu\text{L}/\text{min}$. The total amount of ^{10}B administered to each rat was 20 μg . We then assayed the ^{10}B concentration of tumor, blood, and normal brain by inductively coupled plasma-atomic emission spectrometry. In this study, we sampled normal tissues from both

TABLE 1. Boron Concentrations in Brain Tumors in Rats Bearing F98 Gliomas to Which Polyethylene Glycol Liposome (Sodium Borocaptate, Iomeprol) or Transferrin-Conjugated Polyethylene Glycol Liposome (Sodium Borocaptate, Iomeprol) Was Administered by Convection-Enhanced Delivery^a

BDS	Time, h ^b	Boron Concentration, $\mu\text{g/g}$				Tumor Brain Ratio	
		Tumor	Brain Ipsilateral	Brain Contralateral	Blood	Ipsilateral Normal Brain	Contralateral Normal Brain
PEG liposome (BSH, Iomeprol)	0 ^c	33.5 \pm 10.5	0.6 \pm 0.6	0.3 \pm 0.1	0.4 \pm 0.2	55.8	111.7
	24	22.5 \pm 6.1	1.7 \pm 1.5	1.0 \pm 0.6	0.4 \pm 0.1	13.2	22.5
	48	8.5 \pm 7.9	1.5 \pm 0.7	0.4 \pm 0.3	0.4 \pm 0.1	5.7	21.3
	72	4.9 \pm 4.6	0.2 \pm 0.1	0.2 \pm 0.1	0.5 \pm 0.2	24.5	24.5
TF-PEG liposome (BSH, Iomeprol)	0 ^c	55.2 \pm 26.6	2.1 \pm 2.5	0.4 \pm 0.2	0.6 \pm 0.3	26.3	138.0
	24	82.2 \pm 18.6	0.7 \pm 0.4	0.3 \pm 0.2	0.6 \pm 0.1	117.0	274.0
	48	41.2 \pm 14.4	1.2 \pm 1.0	0.9 \pm 0.6	0.9 \pm 0.1	34.3	45.8
	72	25.8 \pm 13.5	0.4 \pm 0.2	0.4 \pm 0.2	0.6 \pm 0.2	64.5	64.5

^aEach point represents the mean \pm standard deviation. BDS, boron delivery system; PEG, polyethylene glycol; BSH, sodium borocaptate; TF-PEG, transferrin-conjugated polyethylene glycol.

^bHours after convection-enhanced delivery of each BDS.

^cThe time point of 0 means the point just after rats were killed.

hemispheres and defined the normal tissue from the tumor-bearing hemisphere as ipsilateral normal brain and the normal tissue from the other hemisphere as contralateral normal brain. The normal brain of the ipsilateral side, at least a couple of millimeters away from the tumor

border, was sampled with approximately 1 g for ¹⁰B content measurement. The normal brain of the contralateral side, symmetrical for the ipsilateral sampling, was sampled for the measurement.

Imaging Study

For the imaging study, at selected times (0, 24, 48, and 72 hours) after termination of CED, rats were analyzed by CT to evaluate the distribution of BDS and were then euthanized. In this study, we used a high-speed helical CT imaging system (Aquilion 64; Toshiba Medical Systems, Tochigi, Japan). Real-time coronal CT scans (1-mm slice thickness, 1-mm spacing) were performed. We also did a covisualization study using iodine contrast agent (Iomeprol) and fluorescence dye, co-encapsulated into the TF-PEG liposome infused by CED with the CT scan the same as for BDS.

All procedures were performed according to the Osaka Medical College Regulations on Animal Experimentation.

Statistical Analysis

Pairwise comparisons were conducted using Student's *t* test. Group differences resulting in *P* values of $<.05$ were considered statistically significant.

RESULTS

Evaluation of the Normal Rat Brain Infused BDS by CED

Fischer 344 rats receiving a 20- μg ¹⁰B infusion of PEG liposome (BSH, Iomeprol) or TF-PEG liposome (BSH, Iomeprol) by CED into their right hemisphere showed no substantial evidence of adverse effects over a 14-day period. Daily observations revealed no clinical deficits during the study. The rats appeared healthy and gained or maintained body weight at the same rate as did normal rats. Histological evaluation from a representative rat euthanized on day 7 after infusion revealed some evidence of

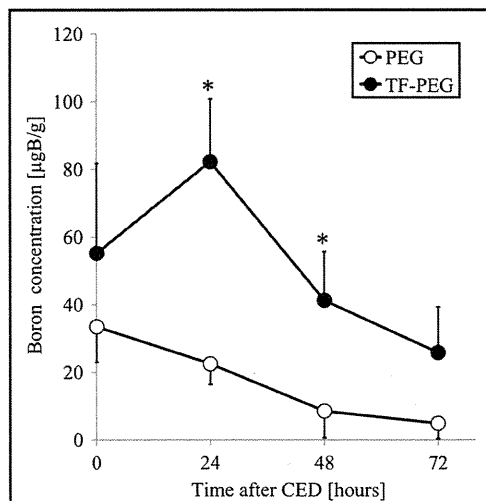


FIGURE 2. Boron concentration of the tumor at selected times after convection-enhanced delivery (CED) administration of each boron delivery system, polyethylene glycol (PEG) liposome (sodium borocaptate [BSH], Iomeprol) or transferrin-conjugated polyethylene glycol (TF-PEG) liposome (BSH, Iomeprol). The TF-PEG group (●) and the PEG group (○). At all the time points, the tumor boron concentration in the TF-PEG group was higher than that in the PEG group. Especially at 24 and 48 hours after CED, the boron concentrations in the TF-PEG group were significantly higher than those in the PEG group ($P < .05$).

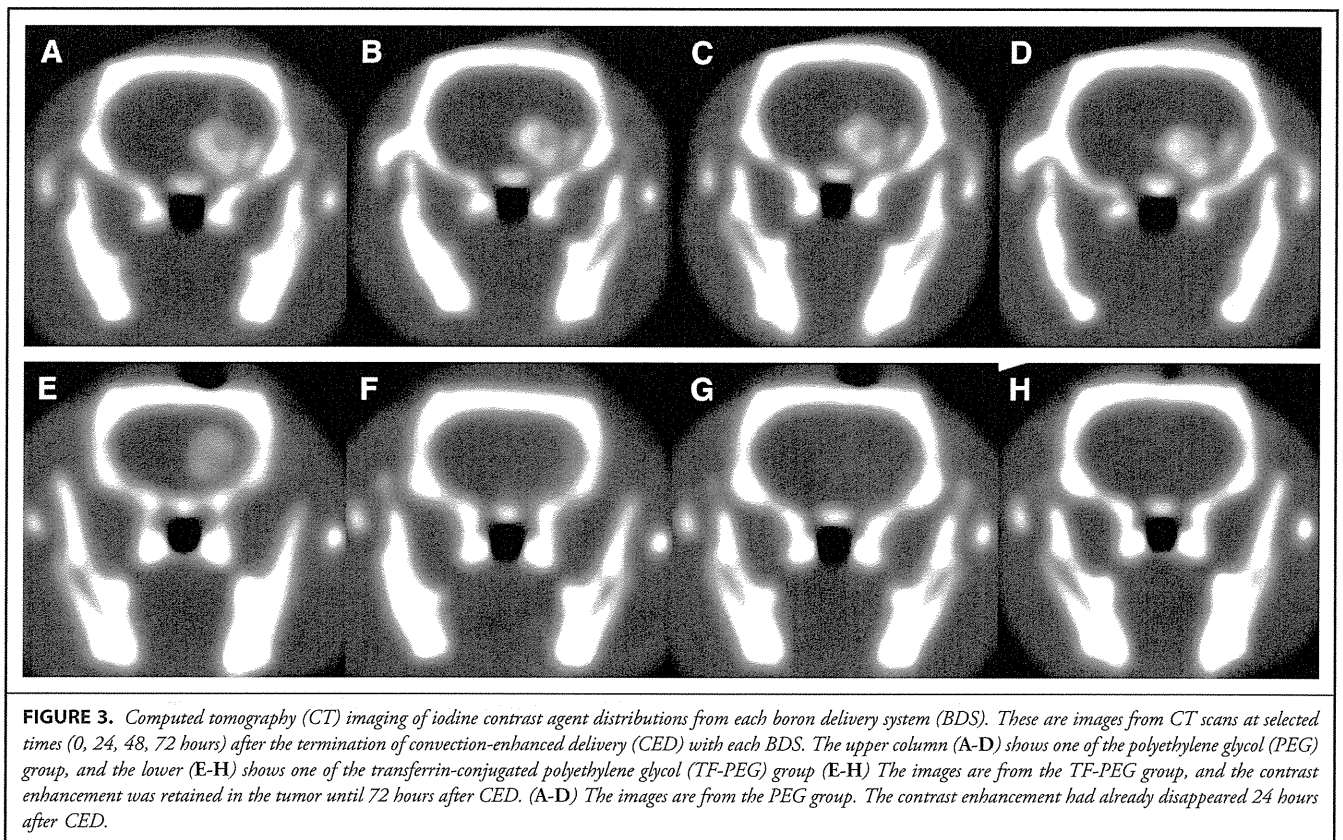


FIGURE 3. Computed tomography (CT) imaging of iodine contrast agent distributions from each boron delivery system (BDS). These are images from CT scans at selected times (0, 24, 48, 72 hours) after the termination of convection-enhanced delivery (CED) with each BDS. The upper column (A-D) shows one of the polyethylene glycol (PEG) group, and the lower (E-H) shows one of the transferrin-conjugated polyethylene glycol (TF-PEG) group (E-H). The images are from the TF-PEG group, and the contrast enhancement was retained in the tumor until 72 hours after CED. (A-D) The images are from the PEG group. The contrast enhancement had already disappeared 24 hours after CED.

tissue inflammation in the striatal regions proximal to the needle track on the site. This tissue reaction was observed only adjacent to the needle tract (data not shown).

In Vitro Uptake Study

The boron concentrations of F98 glioma cells 6 hours after exposure to TF-PEG liposome (BSH, Iomeprol) were significantly higher than those after exposure to PEG liposome (BSH, Iomeprol): 51.9 ± 6.8 and 16.1 ± 4.8 $\text{ng}^{10}\text{B}/10^6$ cells, respectively. (Figure 1) ($P < .05$).

F98 glioma line showed the minimum accumulation of BSH by TF-PEG liposomes among other glioma lines (C6, U251, U87MG, and U118MG).

In Vivo Biodistribution Study

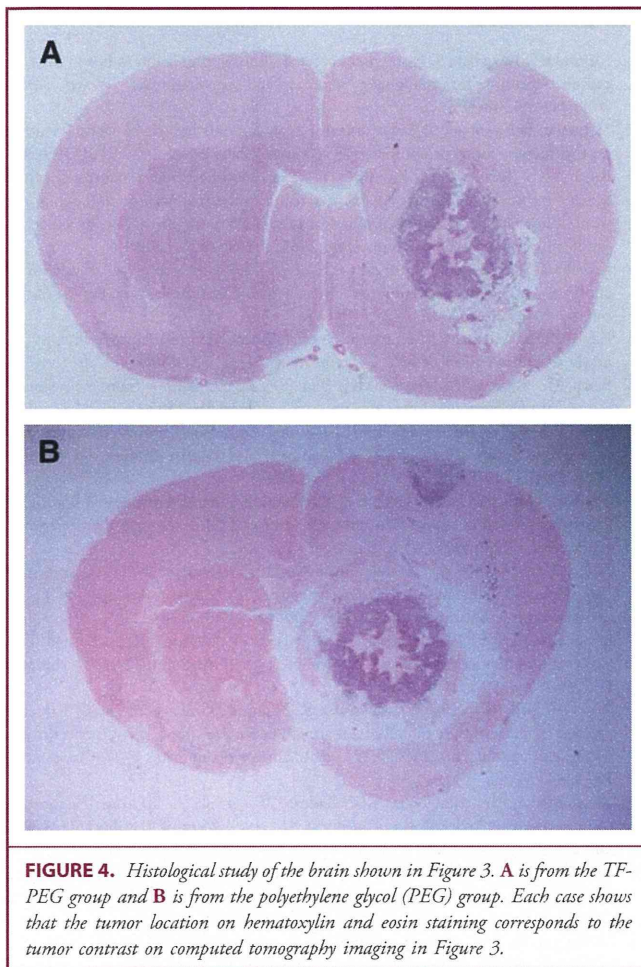
Table 1 summarizes the biodistribution data for PEG liposome (BSH, Iomeprol) and TF-PEG liposome (BSH, Iomeprol) after CED administration to rats bearing F98 brain tumors. The boron concentrations in tumors were significantly higher in the TF-PEG group than in the PEG group at 24 and 48 hours after CED (Figure 2) ($P < .05$). Especially at 24 hours after CED, the TF-PEG group showed a higher mean tumor boron concentration (82.2 ± 18.6 $\mu\text{g}^{10}\text{B}/\text{g}$) and a higher tumor-to-normal brain ratio

(274). On the other hand, at that time point, the boron concentrations of blood and contralateral normal brain were less than 1.0 $\mu\text{g}^{10}\text{B}/\text{g}$. In addition, the boron concentrations in the other organs such as liver, spleen, kidney, heart, lung, muscle, and skin were also less than 1.0 $\mu\text{g}^{10}\text{B}/\text{g}$ (data not shown).

Imaging Study

Figures 3 and 4 show the results of the imaging study by CT and histological study of the brain from same rats, respectively, at 4 time points (0, 24, 48, and 72 hours). The CT images showed that the contrast enhancement of the tumor in the TF-PEG group was retained for at least until 72 hours after CED, whereas in the PEG group, the enhancement had already disappeared by 24 hours after CED. The mean Hounsfield unit values in the PEG group and the TF-PEG group were 269 ± 33.3 and 281 ± 88.4 , respectively, at 0 hours, and 142 ± 40.6 and 256 ± 39.2 , respectively, at 24 hours ($P < .05$) (Figure 5).

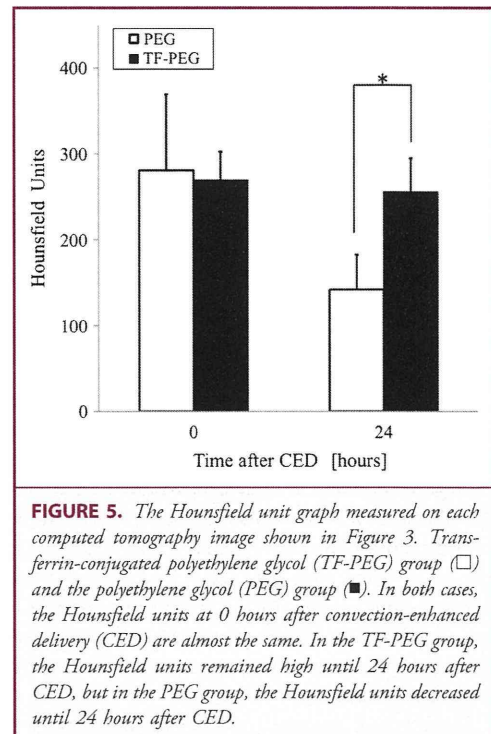
In the covisualization study using iodine contrast agent (Iomeprol) and fluorescence dye, co-encapsulated into the TF-PEG liposome administered by CED shows compatible distribution of both agents (left, fluorescence photography; right, CT scan) (see Figure, Supplemental Digital Content 1, <http://links.lww.com/NEU/A371>).



DISCUSSION

We previously reported that significantly higher concentrations of ^{10}B in tumor tissues in U87 Δ brain tumor-bearing nude mice were achieved with systemic TF-PEG liposome (BSH) administration compared with mice administered PEG liposome (BSH) or bare BSH.⁹ However, the results of that study led us to speculate on 2 problems: the limitation on ^{10}B accumulation because of the BBB, especially in the microscopic tumor cell invasion area, and the unexpected accumulation into other organs. In this study, to overcome these problems, we devised a combination of tumor targeting by transferrin and CED as a method for local drug injection directly into the brain independent of the BBB. Moreover, we devised a novel liposomal BDS that contained Iomeprol as an iodine contrast agent simultaneously with BSH to visualize the distribution of these BDSs in the brain by using CT.

The results of this *in vitro* boron uptake study confirmed that TF-PEG liposome can deliver BSH into F98 cells efficiently. As for the *in vivo* biodistribution study, we found that TF-PEG



liposome can also accumulate ^{10}B at significantly high concentrations in the tumor tissue by CED, whereas low ^{10}B concentrations are maintained in normal brain, blood, and other organs. Neutron irradiation is expected to provide immeasurable tumor control efficacy by virtue of this enormously higher contrast in ^{10}B concentration to the normal brain, allowing decreased irradiation doses to the surrounding normal tissues. F98 glioma cell line showed the minimum accumulation of BSH by TF-PEG liposomes among 5 glioma cell lines tested in this study. Therefore, if we use other cell lines *in vivo* study, more promising results may be expected.

CED itself is a less invasive procedure, and Lonser et al²¹ reported that histological inflammation was typical only within a 50- μm radius of the catheter if the agent infused was nontoxic. They also reported that CED had been proved safe in a number of species, ranging from mice to humans, and did not produce cerebral edema or measurably increased intracranial pressure. On the other hand, Saito et al¹³ reported that a heterogeneous tissue arrangement of the tumor gives rise to an irregular distribution of the infused agent and to leakage into undesirable areas. They also mentioned that ideal and expected tissue distribution after CED can be significantly decreased when the catheter tip is placed near a large blood vessel, white matter tracts, or the resection cavity because of fluid escaping along the path of least resistance.

Thus, the idea of using imaging to visualize locally injected agents would logically arise. We devised a novel liposomal BDS containing Iomeprol, an iodine contrast agent, simultaneously

with BSH. Using imaging technology, such as CT, this liposomal BDS was successfully visualized and its distribution was well recognized on CT imaging even when injected into the small brain of the rat by CED.

In BNCT, unlike other therapies with cytotoxic agents such as targeted toxins²² or anticancer drugs, the infused agent itself has no cytotoxicity until neutron irradiation is applied. So if some technical errors, such as those that Saito et al mentioned, in CED were revealed on a CT image (eg, an undesirable distribution of BDS that leaked into the cerebral ventricle or subarachnoid space), neutron irradiation could be postponed so that the safety of the therapy would be ensured. Rousseau et al¹⁹ reported the efficacy of an iodine tracer not only as a tumor contrast agent on CT imaging but also as a dose-enhancement agent for synchrotron stereotactic radiotherapy. Their method also required precise tumor targeting, so they should have encountered the same problems as those in our study with regard to BNCT. They also adopted CED to improve iodine distribution for synchrotron stereotactic radiotherapy treatment and mentioned that its efficacy and safety in that CED can achieve high iodine concentrations in the target area and low iodine concentrations in the surrounding healthy brain tissues and blood vessels. With or without cytotoxicity of the infused agent, visualization through clinical imaging is essential for the treatment of malignant brain tumors.

In the current study, some problems arose. First, it has not been solved how the infused BDSs, liposomes, and encapsulated BSH and Iomeprol were metabolized. In Figures 2 and 4, ¹⁰B concentration in tumor tissue is not proportional to Hounsfield unit value at the concerned time. This shows that there is a difference in behavior after injection between BSH and Iomeprol. If the metabolic kinetics of the BDS were disclosed, it would enable us to evaluate the ¹⁰B concentration in tumor tissue by CT and Hounsfield unit value. We overcame one of the important problems of CED that caused undesirable distribution of the BDS, such as leaking into the cerebral ventricle or subarachnoid space, by co-encapsulation with drug and contrast agent for CT imaging. However, distribution of the BDS was accurately tracked by the CT imaging. Second, we could not apply neutron irradiation to evaluate the true toxicity and the therapeutic efficacy of this BDS in the current study because both reactors (KUR and JRR4) in Japan had been unavailable because of repairs and the change to uranium as fuel.

In the next step of our work, we expect to confirm that our novel strategy can obtain higher efficacy in BNCT.

Disclosure

This work was supported by Grants-in-Aid for Scientific Research for Young Scientists (B) (18791030 to S.K. and 20791022 to N.I.), by Grants-in-Aid for Scientific Research (C) (20591728 to S.K.) and (B) (19390385 to S.I.M.) from the Japanese Ministry of Education, Culture, Sports, Science and Technology, and by the Eisai Science Foundation to S.K. This work was also supported in part by the Takeda Science Foundation for Osaka Medical College. The authors have no personal financial or institutional interest in any of the drugs, materials, or devices described in this article.

REFERENCES

- Miyatake S, Kawabata S, Nonoguchi N, et al. Pseudoprogression in boron neutron capture therapy for malignant gliomas and meningiomas. *Neuro Oncol*. 2009;11(4):430-436.
- Miyatake S, Kawabata S, Yokoyama K, et al. Survival benefit of Boron neutron capture therapy for recurrent malignant gliomas. *J Neurooncol*. 2009;91(2):199-206.
- Miyatake S, Kawabata S, Kajimoto Y, et al. Modified boron neutron capture therapy for malignant gliomas performed using epithermal neutron and two boron compounds with different accumulation mechanisms: an efficacy study based on findings on neuroimages. *J Neurosurg*. 2005;103(6):1000-1009.
- Kawabata S, Miyatake S, Kajimoto Y, et al. The early successful treatment of glioblastoma patients with modified boron neutron capture therapy. Report of two cases. *J Neurooncol*. 2003;65(2):159-165.
- Kawabata S, Miyatake S, Kuroiwa T, et al. Boron neutron capture therapy for newly diagnosed glioblastoma. *J Radiat Res (Tokyo)*. 2009;50(1):51-60.
- Barth RF, Coderre JA, Vicente MG, Blue TE. Boron neutron capture therapy of cancer: current status and future prospects. *Clin Cancer Res*. 2005;11(11):3987-4002.
- Wei Q, Kullberg EB, Gedda L. Trastuzumab-conjugated boron-containing liposomes for tumor-cell targeting; development and cellular studies. *Int J Oncol*. 2003;23(4):1159-1165.
- Yang W, Barth RF, Adams DM, et al. Convection-enhanced delivery of boronated epidermal growth factor for molecular targeting of EGF receptor-positive gliomas. *Cancer Res*. 2002;62(22):6552-6558.
- Doi A, Kawabata S, Iida K, et al. Tumor-specific targeting of sodium borocaptate (BSH) to malignant glioma by transferrin-PEG liposomes: a modality for boron neutron capture therapy. *J Neurooncol*. 2008;87(3):287-294.
- Bobo RH, Laske DW, Akbasak A, Morrison PF, Dedrick RL, Oldfield EH. Convection-enhanced delivery of macromolecules in the brain. *Proc Natl Acad Sci U S A*. 1994;91(6):2076-2080.
- Wu G, Barth RF, Yang W, Kawabata S, Zhang L, Green-Church K. Targeted delivery of methotrexate to epidermal growth factor receptor-positive brain tumors by means of cetuximab (IMC-C225) dendrimer bioconjugates. *Mol Cancer Ther*. 2006;5(1):52-59.
- Mukundan S Jr, Ghaghada KB, Badea CT, et al. A liposomal nanoscale contrast agent for preclinical CT in mice. *AJR Am J Roentgenol*. 2006;186(2):300-307.
- Saito R, Bringas JR, McKnight TR, et al. Distribution of liposomes into brain and rat brain tumor models by convection-enhanced delivery monitored with magnetic resonance imaging. *Cancer Res*. 2004;64(7):2572-2579.
- Dickinson PJ, LeCouteur RA, Higgins RJ, et al. Canine model of convection-enhanced delivery of liposomes containing CPT-11 monitored with real-time magnetic resonance imaging: laboratory investigation. *J Neurosurg*. 2008;108(5):989-998.
- Aoki I, Bakalova R. MR molecular imaging using drug delivery system. *Drug Delivery System*. 2008;23(1):61-68.
- Weaver M, Laske DW. Transferrin receptor ligand-targeted toxin conjugate (Tf-CRM107) for therapy of malignant gliomas. *J Neurooncol*. 2003;65(1):3-13.
- Murad GJ, Walbridge S, Morrison PF, et al. Real-time, image-guided, convection-enhanced delivery of interleukin 13 bound to pseudomonas exotoxin. *Clin Cancer Res*. 2006;12(10):3145-3151.
- Vogelbaum MA. Convection enhanced delivery for the treatment of malignant gliomas: symposium review. *J Neurooncol*. 2005;73(1):57-69.
- Rousseau J, Boudou C, Esteve F, Elleaume H. Convection-enhanced delivery of an iodine tracer into rat brain for synchrotron stereotactic radiotherapy. *Int J Radiat Oncol Biol Phys*. 2007;68(3):943-951.
- Maruyama K, Ishida O, Kasaoka S, et al. Intracellular targeting of sodium mercaptoundecahydrododecaborate (BSH) to solid tumors by transferrin-PEG liposomes, for boron neutron-capture therapy (BNCT). *J Control Release*. 2004;98(2):195-207.
- Lonser RR, Walbridge S, Garmestani K, et al. Successful and safe perfusion of the primate brainstem: in vivo magnetic resonance imaging of macromolecular distribution during infusion. *J Neurosurg*. 2002;97(4):905-913.
- Rainov NG, Soling A. Clinical studies with targeted toxins in malignant glioma. *Rev Recent Clin Trials*. 2006;1(2):119-131.

Supplemental digital content is available for this article. Direct URL citations appear in the printed text and are provided in the HTML and PDF versions of this article on the journal's Web site (www.neurosurgery-online.com).

Acknowledgments

We thank Dr Rolf F. Barth, Department of Pathology, The Ohio State University, for preparing the F98 cell line and Hitomi Kuroda for technical assistance.

COMMENTS

The authors report a novel means to introduce potential sensitizing agents into an experimental brain tumor in an animal model using convection-enhanced delivery. The goal is to introduce these potential agents into the brain surrounding a tumor mass and eventually administer neutron radiation with the hope of providing greater cell kill, especially in the infiltrated zone. In essence, this is a study showing that specially tailored pharmaceuticals can be created to increase delivery of a selected agent in the target zone and that addition of other agents may make recognition of the target by imaging possible as well. It would be even better to demonstrate in a part 2 study that this targeting of sensitizing compounds actually resulted in a therapeutic response using boron neutron capture therapy (BNCT). This technology has been advocated in a relatively few centers for more than 40 years; perhaps because of the large overhead cost and lack of major therapeutic safety window, it has never reached mainstream use. Further efforts may allow safer BNCT, especially because the authors show that tissue concentrations are significantly reduced in other tissues, an important feature that may improve the safety of BNCT during the actual radiation administration. The risk-benefit ratio in BNCT has been difficult to ascertain. In the past, neutron radiation was effective at killing the target

tumor but usually resulted in unacceptable radiation toxicity in the brain. Perhaps further efforts in this field will yet allow a beneficial therapeutic window to emerge.

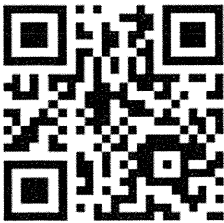
L. D. Lunsford
Pittsburgh, Pennsylvania


The authors describe their early preclinical findings (in vitro and in vivo) in a potentially interesting application and modification of BCNT. Their strategy directly targets glioma cells (and the surrounding region) with transferrin bound to a polyethylene glycol liposome that encapsulates sodium borocaptate and an iodine contrast agent (used for tracking the liposome distribution during computed tomography imaging). To provide high concentrations of this compound to regions in and around glioma, it was delivered to tumor and surrounding region via convection-enhanced delivery.

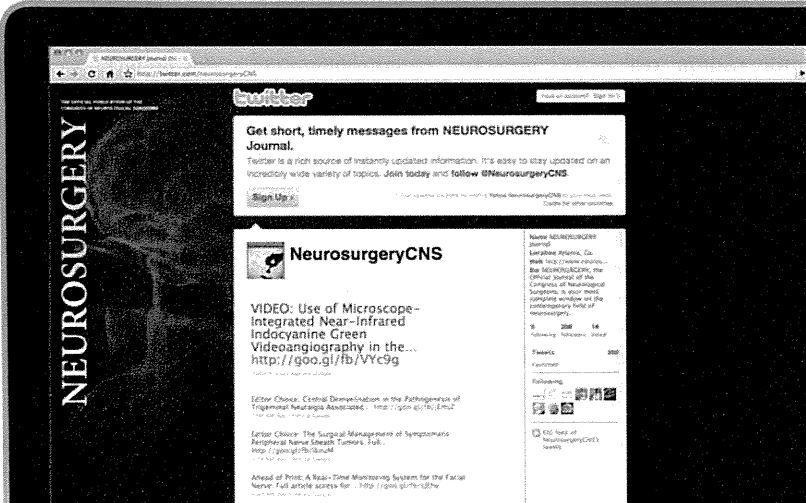
The data from this study indicate that the polyethylene glycol liposome encapsulated sodium borocaptate can be safely and successfully delivered by convection-enhanced delivery in rodent brain tumor models while tracking its distribution using computed tomography imaging. Although these early findings are encouraging from a distribution perspective, the next potential step in determining whether this modification of BCNT for glioma may hold promise will be in determining therapeutic dosing (irradiation) and assessing efficacy in vivo. I look forward to the authors' subsequent work in this area.

Russell R. Lonser
Bethesda, Maryland

Follow NEUROSURGERY® on Twitter







Follow NEUROSURGERY® at <http://www.twitter.com/neurosurgerycns>



ORIGINAL ARTICLE

Hepatocyte growth factor incorporated into herpes simplex virus vector accelerates facial nerve regeneration after crush injury

S Esaki^{1,2}, J Kitoh³, S Katsumi¹, F Goshima², H Kimura², M Safwat¹, K Yamano¹, N Watanabe¹, N Nonoguchi⁴, T Nakamura⁵, RS Coffin⁶, S-I Miyatake⁴, Y Nishiyama² and S Murakami¹

Hepatocyte growth factor (HGF) promotes regeneration of the central nervous system, but its effects on the peripheral nervous system remain unclear. This study was conducted to elucidate the effect of HGF on regeneration of the murine facial nerve after crush injury. To do so, a replication-defective herpes simplex virus vector that incorporated HGF was prepared (HSV-HGF). The main trunk of the facial nerve was compressed by mosquito hemostats, and HSV-HGF, control vector or medium was then applied to the compressed nerve. We found that mice in the HGF group required significantly fewer days for complete recovery from nerve compression. Furthermore, the amplitude of the evoked buccinator muscle compound action potential increased following HSV-HGF application. HGF expression in and around the compressed nerve was demonstrated by enzyme-linked immunoassay and immunohistochemistry. In addition, HSV-HGF introduction around the damaged nerve significantly accelerated recovery of function of the facial nerve. These data suggest a possible role of HGF in promoting facial nerve regeneration after nerve damage. Furthermore, this viral delivery method may be applied clinically for many types of severe facial palsy during facial nerve decompression surgery.

Gene Therapy (2011) 18, 1063–1069; doi:10.1038/gt.2011.57; published online 12 May 2011

Keywords: facial nerve injury; hepatocyte growth factor; HSV

INTRODUCTION

Numerous studies have used the facial nerve axotomy model to investigate the survival-promoting effects of neurotrophic and growth factors on axotomized motor neurons. Ciliary neurotrophic factor was the first factor to demonstrate motor neuronal survival following local application to lesioned axons in the newborn rat.¹ Subsequently, other neurotrophic and growth factors were found to prevent axotomy-induced motor neuron cell death, including neurotrophin-4/5,² insulin-like growth factor-1,³ leukemia inhibitor factor,³ brain-derived neurotrophic factor,⁴ nerve growth factor,⁵ neurotrophin-3 (ref. 6) and glial cell line-derived growth factor.⁷ Although these neurotrophic factors have been shown to promote regeneration of the injured nerve, the functional outcomes have often been limited.^{8,9}

Hepatocyte growth factor (HGF) is a disulfide-linked heterodimeric protein that was initially purified and cloned as a potent mitogen for hepatocytes^{10,11} and a natural ligand for the c-Met protooncogene product.¹² Subsequently, several functions have been ascribed to HGF, including anti-apoptosis, angiogenesis, motogenesis, morphogenesis, hematopoiesis, tissue regeneration in a variety of organs and enhancement of neurite outgrowth.^{13–20} Previous studies have reported that HGF protected neurons from damage and enhanced regeneration in the central nervous system *in vivo*.^{13,19–23} Given the known effects in the literature, HGF is thought to protect neurons from damage and

promote peripheral nerve regeneration; however, little is known about its effects on the peripheral nerve systems.

Herpes simplex virus (HSV) type 1 vectors have been widely used for gene transfer of neurotrophic factors^{24–28} because they are capable of infecting the cells of the nervous system. However, an inherent difficulty with HSV as a vector system lies in disabling the virus from being neurotoxic while maintaining its infection efficiency. To address this problem, we made a replication-defective HSV type 1 vector in which replication was disabled by deleting three critical genes for viral replication.^{29–31} The availability of this vector has already been examined in the nervous system.^{30–32}

In the present study, we incorporated HGF into the replication-defective HSV vector and inoculated murine facial nerves with the vector after compression. Here, for the first time, we demonstrate that HGF prevents peripheral nerve degeneration and promotes regeneration of facial nerve function in a murine model of crush injury.

RESULTS

Time course of facial nerve paralysis after compression

Facial nerve paralysis developed immediately after compression in all mice and then gradually improved and recovered completely by day 14. The time courses of facial scores for mice in each group are shown in Figure 1a. There was no significant difference in final facial scores

¹Department of Otolaryngology, Head and Neck Surgery, Nagoya City University Graduate School of Medical Sciences and Medical School, Nagoya, Japan; ²Department of Virology, Graduate School of Medicine, Nagoya University, Nagoya, Japan; ³Professor Emeritus of Nagoya University School of Medicine, Nagoya, Japan; ⁴Department of Neurosurgery, Osaka Medical College, Osaka, Japan; ⁵Division of Molecular Regenerative Medicine, Osaka University Graduate School of Medicine, Osaka, Japan and ⁶Department of Molecular Pathology in Windeyer Institute of Medical Sciences of University College, London, UK

Correspondence: Dr S Esaki, Department of Otolaryngology, Head and Neck Surgery, Nagoya City University Graduate School of Medical Sciences and Medical School, Kawasumi 1, Mizuho-ku, Nagoya 467-8602, Japan.

E-mail: sesaki@med.nagoya-cu.ac.jp

Received 13 August 2010; revised 19 January 2011; accepted 24 February 2011; published online 12 May 2011

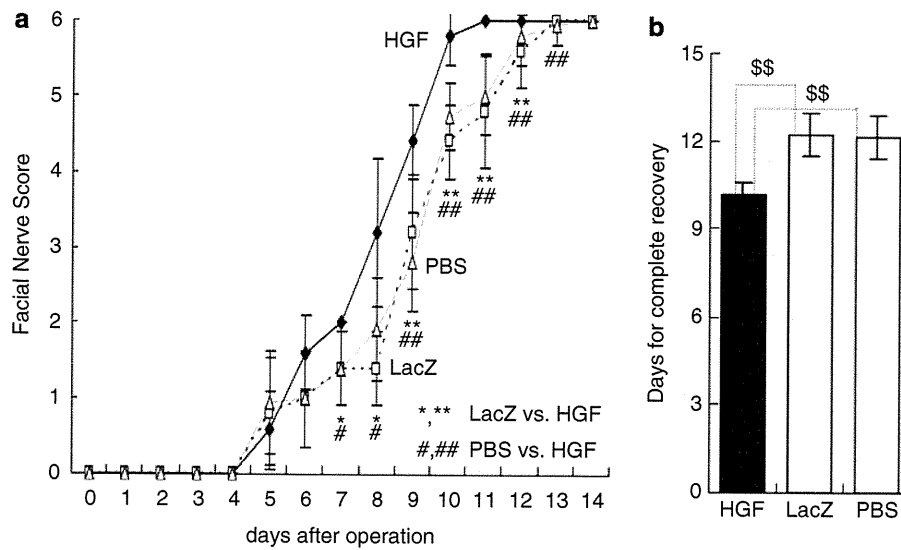


Figure 1 HSV-HGF enhances recovery after crush injury. (a) Time course of facial nerve scores in the HGF ($n=5$), LacZ ($n=5$) and PBS ($n=15$) groups. Error bars indicate standard deviation. Mice in the LacZ and PBS groups showed almost the same degree of recovery, whereas mice in the HGF group showed significantly improved recovery (*, # $P<0.05$; **, ## $P<0.01$). (b) Days required for complete recovery. Mice in the HGF group required significantly fewer days to recover (\$ $P<0.01$). Error bars indicate standard deviation.

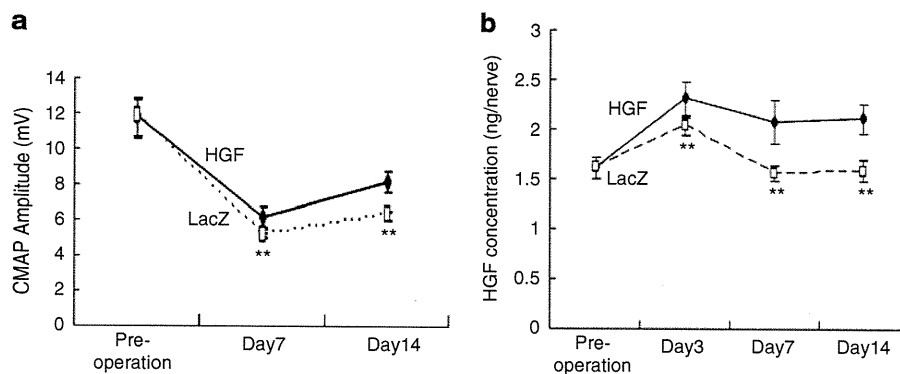


Figure 2 (a) Evoked buccinator muscle CMAP amplitude also showed accelerated recovery. Mean amplitude for the HGF group was significantly greater than that for the LacZ groups on days 7 and 14 (** $P<0.01$). Error bars indicate standard deviation. (b) HGF was detected from the extracts of murine facial nerve. The amount of HGF in the HGF group was greater than that in the LacZ group on days 3, 7 and 14 (** $P<0.01$). Error bars indicate standard deviation.

on day 14 between mice in the LacZ and PBS groups. However, the facial scores for mice in the HGF group on days 7–12 were significantly higher than the scores for mice in the PBS and LacZ groups. We compared the number of days required to reach a score of 6, which indicates complete recovery from facial paralysis. The PBS group required 11.5 ± 0.9 days, the LacZ group required 11.6 ± 1.0 days and the HGF group required 10.3 ± 0.5 days (Figure 1b). Recovery from facial nerve paralysis in the HGF group was significantly faster than in either the LacZ or the PBS groups ($P<0.01$, unpaired t -test). No mice died or showed any significant weight loss or other complications during this experiment.

Electrophysiological examination

The mean evoked compound muscle action potentials (CMAPs) amplitude of the buccinator muscle was 11.8 ± 1.1 mV in both groups combined before nerve compression. On day 7, CMAP amplitude decreased to 5.2 ± 0.3 mV (44%) in the LacZ group and 6.2 ± 0.6 mV (53%) in the HGF group (Figure 2a). The decrease in CMAP

amplitude was significantly larger ($P<0.01$, unpaired t -test) for the LacZ group than the HGF group. However, CMAP amplitudes increased between days 7 and 14 in both the LacZ and HGF groups. On day 14, the CMAP amplitude was 6.3 ± 0.3 mV (53%) in the LacZ group and 8.2 ± 0.6 mV (70%) in the HGF group. Furthermore, the HGF group showed significantly greater recovery of CMAP amplitude compared with the LacZ group ($P<0.01$, unpaired t -test). Finally, the difference in CMAP amplitudes between the HGF group and the LacZ group was larger on day 14 than on day 7.

HGF secretion in nerve extracts

The amount of HGF in the facial nerve before surgery was 1.62 ± 0.11 ng (Figure 2b). HGF in the LacZ group increased to 2.03 ± 0.95 ng on day 3 following surgery, then decreased to 1.56 ± 0.09 ng on day 7. HGF levels showed no significant differences on days 7–14 (1.59 ± 0.11 ng measured on day 14). On the other hand, the HGF level in the HGF group increased to 2.31 ± 0.16 ng on day 3 and then decreased slightly to 2.08 ± 0.21 ng on day 7. This level was

maintained until day 14 (2.11 ± 0.14 ng). Furthermore, HGF levels in the HGF group were significantly higher than levels in the LacZ group between days 3 and 14 ($P < 0.01$, unpaired *t*-test).

Expression of reporter protein (KT3) in the facial nerve's compressed region and nucleus

KT3, a reporter protein of HSV-HGF, was detected in the crushed area of the facial nerve on days 3 (Figure 3a), 7 (Figure 3b) and 14 (Figure 3c) in the HGF group. Transfected cells in the facial nerve were identified as Schwann cells by immunohistochemical and Klüver-Barrera staining of serial sections. Furthermore, we performed dual immunofluorescent staining with a marker for Schwann cells (S-100) and a reporter protein of HSV-HGF (KT-3) to confirm the colocalization of transfected cells and Schwann cells (Figure 3h) in frozen sections on day 14. KT3 antigen (Figure 3g) was detected in Schwann cells. Merged images (Figure 3i) indicated that Schwann cells, which were identified by anti-S-100 antibody, were transfected. In contrast, KT3 was not detected in the facial nerve nucleus (Figure 4b). In addition, neurons showed no morphological changes following compression (Figure 4a).

Degeneration and regeneration of nerve fibers

Most myelinated nerve fibers showed vacuuous changes, but some nerve fibers remained intact in both the HGF and LacZ groups on day 3 (Figures 5a and d). In addition, the number of demyelinated fibers was greater in the HGF group (152 ± 14.6 fibers per mm^2) than in the LacZ group (58 ± 10.1 fibers per mm^2) on day 3. However,

regenerating nerve fibers were seen on days 7 and 14. Furthermore, on days 7 (Figures 5b and e) and 14 (Figures 5c and f), the number of myelinated nerve fibers was greater in the HGF group (276 ± 58.6 fibers per mm^2 on day 7 and 298 ± 53.6 fibers per mm^2 on day 14) than in the LacZ group (164 ± 24.9 fibers per mm^2 on day 7 and 218 ± 47.3 fibers per mm^2 on day 14).

DISCUSSION

Neurotrophic factors have been proposed to be ideally suited for the treatment of neurodegenerative diseases, neuropathies and peripheral nerve injury.³³ However, administration of a growth factor into the body in solution form is not expected to be efficacious for tissue regeneration because of the short half-lives of growth factors. Hence, administration strategies should be based on transfer of genes, molecules or cells into the nervous system. Herpes simplex virus expressing nerve growth factor can be injected directly into the nerve and retrograde transported to mimic the physiological role of the neurotrophin coded for. This method has been shown to prevent the decrease in tyrosine hydroxylase activity seen in sympathetic ganglia after axotomy.³⁴ Similarly, administration of ciliary neurotrophic factor and brain-derived neurotrophic factor transduced in adenoviruses promotes the survival of neonatally axotomized motor neurons.³⁵ Although these experimental strategies were still in the early stages of development at the time of this study, they have demonstrated the potential of genetic manipulation for therapeutic application in the peripheral and central nervous system. Furthermore, these experiments demonstrated the possibility of modifying

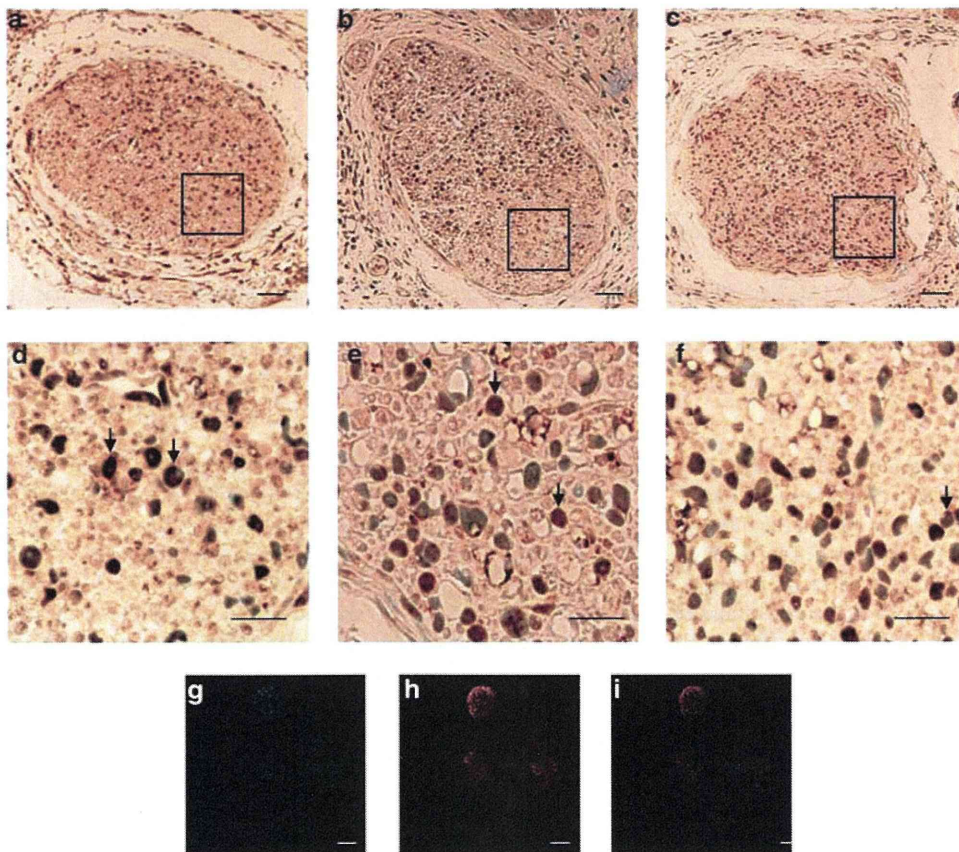


Figure 3 Images of the right facial nerve of the HGF group. The facial nerve and surrounding tissues were stained for KT3 using the immunohistochemical staining on days 3 (a), 7 (b) and 14 (c). Brown cells express the KT3 antigen in and around the facial nerves. Magnifications of the upper row images (a, b and c) are shown in the lower row (d, e and f, respectively). Black arrows indicate the KT3 antigen in the facial nerve. Dual-immunostained images with KT3 antigen (g) and S-100 (h). Merged image (i) shows colocalization of transfected cells and Schwann cells. Scale bars represent 100 μm (a-f), and 10 μm (g-i).

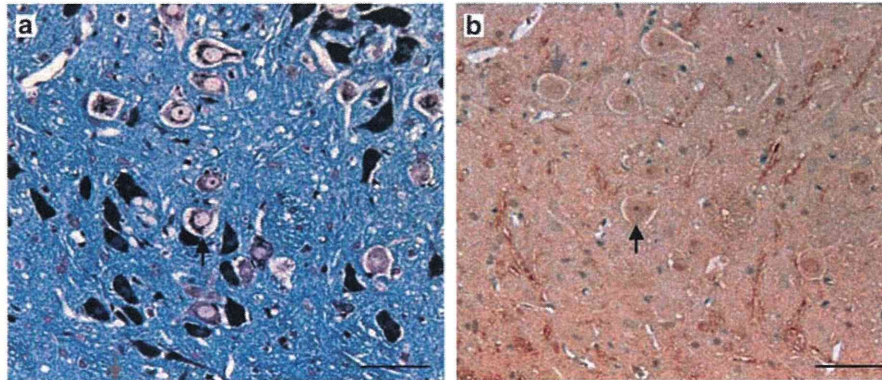


Figure 4 Images of the right facial nucleus of the HGF group. Facial nuclei were stained using the Klüver–Barrera method (a) and stained for KT3 using immunohistochemical staining (b) on day 7. Black arrow shows the facial nucleus, but the KT3 antigen was not detected on day 7. Scale bars represent 100 μ m.

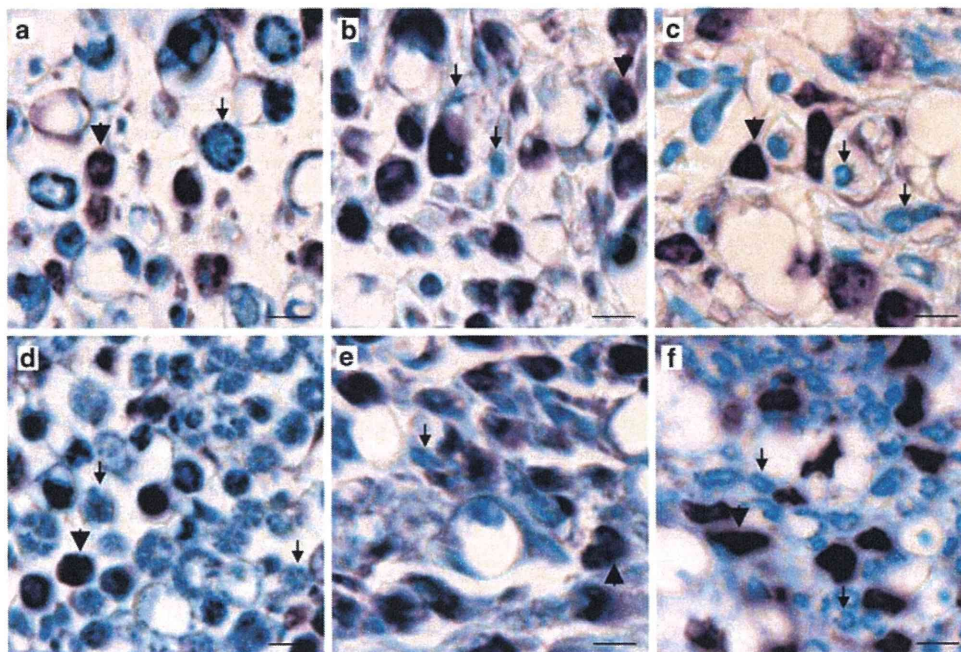


Figure 5 Magnified images of the right facial nerves of both groups, which were stained using the Klüver–Barrera method. The top row shows images from the LacZ group on days 3 (a), 7 (b) and 14 (c), and the bottom row shows images from the HGF group on days 3 (d), 7 (e) and 14 (f). On day 3, bulking myelin (arrows) was seen in the HGF group but not in the LacZ group. Almost all the myelin had degraded by day 7 for both groups, but some myelin regenerated in the HGF group. On day 14, more myelin (arrows) was regenerated in the HGF group than in the LacZ group. Schwann cells (arrowheads) were seen on days 3, 7 and 14 in both groups. Scale bars represent 10 μ m.

neuronal physiology *in vivo* by augmenting the expression and delivery of a critical gene product to neural cells when growth factors are needed.

In the present study, we investigated the effect of HSV-HGF on crush nerve injury by compressing the facial nerve trunk. Previous studies have shown that, in murine models of facial nerve crush injury, reinnervation required 2 weeks,^{36–38} which supports our findings. All mice recovered completely because nerve crush injury is a milder form of lesion than nerve transection and repair or avulsion with neurectomy. The pathophysiology of this nerve crush model was evaluated by facial movement score and CMAP. Facial movements were absent until day 4 and then recovered gradually by day 14. Therefore, the former period was the paralyzed phase, and the latter period was the recovery phase. CMAP amplitude was a quantitative indicator for evaluating Wallerian degeneration of the nerve after injury, as

demonstrated by Esslen.³⁹ CMAPs on day 7 indicated that nerve degeneration was not completed and that functional nerve fibers still remained in both the LacZ and HGF groups. Histopathological findings also supported the presence of a mixture of intact, demyelinated and denervated fibers in the facial nerve trunk. Nerve degeneration on day 7 in the HGF group was less than in the LacZ group; CMAP amplitude was reduced to 56% in the LacZ group and 47% in the HGF group, suggesting that HGF prevented nerve degeneration. The difference in CMAP amplitudes between the LacZ and HGF groups was greater on day 14 (1.9 mV) than on day 7 (1.0 mV). This difference is thought to be attributed to the effect of HGF during nerve regeneration. Therefore, CMAP findings suggested that HGF affected the facial nerve by preventing degeneration and promoting regeneration. The CMAP amplitude did not recover to the preoperative level, although facial nerve paralysis recovered completely by day 14. This

finding indicates that normal facial function can be restored without complete regeneration of the nerve fibers. A similar discrepancy between CMAP amplitude and recovery of facial nerve paralysis in the recovery phase was also reported in a mouse model of HSV neuritis⁴⁰ and in a human study of Bell's palsy.⁴¹

Wild-type HSV type 1 is known to have affinity for neurons of the facial nerve and cause pathology in an animal model,⁴² and the majority of Bell's palsy is caused by reactivation of HSV type 1 latently infected in the geniculate ganglion.⁴³ Therefore, the question facing gene transfer using the HSV vector is how to transfer genes effectively while avoiding neuropathogenesis. In this study, we negated its neuropathogenesis by deleting the genes encoding $\alpha 4$ and VP16, which are necessary for initiating viral replication, and $\gamma_1 34.5$, which is a prerequisite for neuropathogenicity of HSV.⁴⁴ There are two methods for promoting regeneration of a crushed peripheral nerve using neurotrophins. One method is to apply the neurotrophins directly to the crushed nerve with bioresorbable materials,^{8,45} and the other method is to transfer genes by means of viral vectors. Other studies using HSV vectors have reported successful transfection of neurotrophins to the peripheral nerve nucleus.^{26,27} These authors disrupted neuropathogenesis of the vectors by deleting the genes encoding $\alpha 4$ and $\alpha 27$, which are essential to neuropathogenesis. However, these authors did not discuss the activity of neurotrophins at the site of the peripheral lesion. The uniqueness of our study came from successful HGF transfection into Schwann cells by directly applying the replication-defective HSV vector onto the crushed nerve. The transfected Schwann cells secreted HGF continuously, and the many known effects of HGF effectively prevented peripheral nerve degeneration and promoted nerve regeneration. HGF in the facial nerve extract increased on day 3 in all groups, including the LacZ group. The timing of the increase of HGF suggests a protective or regenerative function for the peripheral nerve. Although we measured the concentration of HGF over 14 days until the facial nerve recovered completely, another study of spinal cord regeneration, in which the same vector was injected into the spinal cord before compression, showed that the HGF increase was maintained for at least 4 weeks, and better functional recovery was observed.²¹ In spinal cord injury, the mRNA expression levels of HGF and its receptor, c-Met, were reported to be upregulated.²¹ Although we did not investigate the mechanism of how HGF affected the crushed nerve, the HGF-c-Met system seemed to be important for peripheral nerve injury. As further evidence, another mouse model in which incomplete regeneration is observed without treatment should be prepared to show the potential of HSV-HGF.

Collateral axonal branching is inevitable when nerves regenerate after an injury. In our study, axonal branching is thought to occur less often after transection and repair of peripheral nerves because crush injury is a milder lesion. As we did not transect, but crushed, the

nerve, the paths for axon sprouting were preserved. Figure 5 shows the regeneration and formation of axons led by Schwann cells. When we investigate a mouse model of profound nerve injury in the future, marked collateral axonal branching is likely to occur at the site of lesion. Such excessive, redundant axonal branching is a major obstacle to the recovery of co-ordinated muscle function. Therefore, motion analysis is necessary to analyze the movement of the eye and vibrissae in detail to evaluate synkinesis. As mentioned above, another important consideration when using an HSV vector is avoiding neurotoxicity. In our model, cells transfected with HSV-HGF were not found in the facial nucleus, and no mice showed signs of encephalitis or other complications. These observations provide evidence for the safety of our vectors.

In a clinical context, our method can be applied in the treatment of selected patients with severe facial palsy caused by temporal bone fracture, Bell's palsy and Ramsay Hunt syndrome, all of which require decompression surgery. Decompression surgery is performed by opening the bony Fallopian canal, exposing the facial nerve and incising the nerve sheath. HSV-HGF can then easily be applied directly to the exposed injured nerve. However, the effect of decompression itself is limited even if performed with perfect timing. Therefore, application of our vector will likely provide even better surgical outcomes when decompression surgery is required.

MATERIALS AND METHODS

Preparation of HGF viral vector

Replication-defective HSV type 1 vectors were made by deletion of three critical genes for viral replication that encode $\alpha 4$, $\gamma_1 34.5$ and VP16. These vectors contained an HSV latency-associated transcript (LAT) promoter and two enhancer elements, including a cytomegalovirus (CMV) enhancer and Woodchuck posttranscriptional regulatory elements (WPREs) (Figure 6). These vectors coded for LacZ (HSV-LacZ) or rat HGF (HSV-HGF), as described previously.⁴⁶ The former vector contained the CMV enhancer followed by the LacZ sequence, and the latter contained the full-length rat HGF complementary DNA tagged with the KT3 (large T antigen of simian virus 40) epitope. The two viruses were prepared with the same titers (1×10^8 pfu ml⁻¹).

Surgery and viral vector inoculation

Four-week-old specific-pathogen-free female Balb/C mice (14–16 g body weight; CLEA Japan, Inc., Tokyo, Japan) were used throughout this study. All mice were given food and water *ad libitum*. All experiments were approved by the University Committee in accordance with the Guidelines for Animal Experimentation of Nagoya City University (H17-21). Mice were anesthetized by intraperitoneal administration of ketamine (100 mg kg⁻¹) and xylazine (10 mg kg⁻¹). The main trunk of the right facial nerve was exposed below the parotid gland, released from the surrounding connective tissue, and compressed for 30 s using mosquito hemostats with a compression pressure of 6–8 MPa. Successful compression was confirmed by the lack of eye blink and whisker movement after surgery. After the operation, animals were divided into three experimental groups: HGF, LacZ and PBS. For the HGF group, 10 μ l

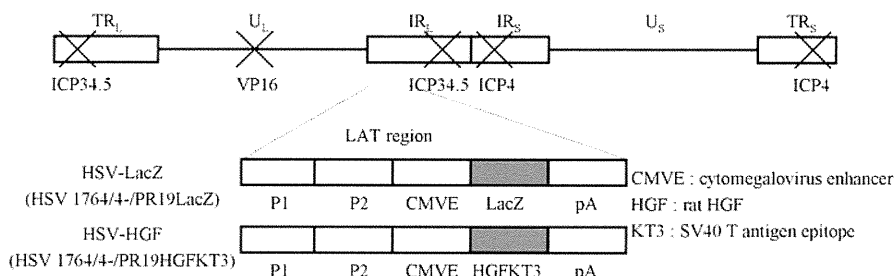


Figure 6 Schematic of HSV vector. Some of the genes required for viral growth *in vitro* (coding ICP4, ICP34.5 and VP16) were disrupted, and HGFKT3 (HGF tagged with KT3) or LacZ was inserted in the latency-associated-transcript (LAT) region.

(10^6 pfu) of HSV-HGF was applied to the compressed nerve. To avoid additional damage, HSV-HGF was carefully applied to the nerve with a micropipette. For the LacZ group, an equal volume of HSV-LacZ (10^6 pfu) was applied to the nerve, and for the PBS group, an equal volume of phosphate-buffered saline (PBS) was applied. Five minutes after virus application, the skin was closed with nylon suture.

Clinical evaluation of facial nerve paralysis

Body weight and clinical signs of facial nerve paralysis were monitored each day following nerve compression. To evaluate facial nerve paralysis, eye blink and whisker movement of each mouse were scored separately as previously described.³⁷ Specifically, for each facial area, a score of 0 was given for no detectable movement, 1 for detectable motion, 2 for significant but asymmetric voluntary motion and 3 for symmetric voluntary motion. Facial nerve function was determined by the total scores for eye blink and whisker movement.

Electrophysiology

CMAPs were evoked using conventional procedures with an electromyography monitor (UA-103U, Unique Medical Co., Ltd, Osaka, Japan) before surgery and on days 7 and 14 following surgery. Under anesthesia, the facial nerve was exposed, bipolar needles were hooked to the main trunk, and the nerve was stimulated supermaximally by single electrical pulses of frequency 1 Hz lasting 5 ms. Response amplitude was measured from peak to trough of the evoked response.

HGF from facial nerve extracts

The concentration of HGF was measured with enzyme-linked immunosorbent assay (ELISA) before surgery and on days 3, 7 and 14 after surgery. Under anesthesia with ketamine and xylazine, 3-mm-long segments of each facial nerve trunk, including the compressed site, were removed. They were rinsed 3 times with PBS, and sonicated in the solution that included 50 mM Tris-HCl, 2 M NaCl, 1% Triton X-100 and Protease Inhibitor Mix (GE Healthcare, Little Chalfont, UK). Thereafter, HGF was measured with rat HGF EIA (Institute of Immunology, Tokyo, Japan), as previously reported.^{19,46} This kit is known to react with mouse HGF because rat HGF has about 90.9% amino-acid sequence homology with mouse HGF.⁴⁷

Expression of the reporter protein around the inoculated nerve and in the facial nucleus

Mice were transcardially perfused with 4% paraformaldehyde under deep anesthesia on day 3, 7 or 14. Following perfusion, the head was removed, decalcified in EDTA and embedded in paraffin. A portion of the facial nerve was obtained 1 mm distal to the compressed site. Sections 3 μ m thick were stained by the Klüber–Barrera method. To detect transfected cells, immunohistochemistry for KT3 was used with a rabbit polyclonal anti-KT3 primary antibody (Bethyl Laboratories Inc., Montgomery, TX, USA) and an Envision+ system (Dako, Glostrup, Denmark) secondary antibody. Antibody binding was visualized by adding the chromogenic indicator dye DAB+ (Dako). Antibody specificity was confirmed using universal negative control rabbit immunoglobulin (Dako). The facial nucleus was also stained with the Klüber–Barrera method and immunohistochemistry staining for KT3. Images of sections were obtained via microscopy (Olympus Co., Ltd, Tokyo, Japan) with a CCD camera (Nikon, Co., Ltd, Tokyo, Japan). Frozen tissues were soaked in 20% sucrose in PBS at 4 °C overnight and frozen at -80°C . Serial sections (12 μ m) were cut using a cryostat. Dual immunofluorescence staining was used to confirm the colocalization of transfected cells and Schwann cells in frozen sections. Rabbit polyclonal anti-S-100 (Thermo Fisher Scientific Inc., Waltham, MA, USA) antibody and mouse monoclonal anti-KT3 antibody (Covance Research Products, Princeton, NJ, USA) were used in combination with Alexa Fluor 488-conjugated goat anti-mouse antibody and 546-conjugated goat anti-rabbit antibody (Invitrogen Corp., Carlsbad, CA, USA).⁴⁸ The images were obtained using confocal laser scanning microscopy (Leica Microsystems GmbH, Wetzlar, Germany).

Statistical analyses

Facial nerve score data were evaluated with Mann–Whitney tests, and other data were evaluated using unpaired *t*-tests in StatView Software (SAS Institute,

Cary, NC, USA). Differences with a probability value of $P < 0.05$ were considered statistically significant.

CONFLICT OF INTEREST

The authors declare no conflict of interest.

ACKNOWLEDGEMENTS

This work was supported by a Grant-in-Aid from the Japan Society for the Promotion of Science (19591984).

- Sendtner M, Kreutzberg GW, Thoenen H. Ciliary neurotrophic factor prevents the degeneration of motor neurons after axotomy. *Nature* 1990; **345**: 440–441.
- Koliatsos VE, Cayouette MH, Berkemeier LR, Clatterbuck RE, Price DL, Rosenthal A. Neurotrophin 4/5 is a trophic factor for mammalian facial motor neurons. *Proc Natl Acad Sci USA* 1994; **91**: 3304–3308.
- Hughes RA, Sendtner M, Thoenen H. Members of several gene families influence survival of rat motoneurons *in vitro* and *in vivo*. *J Neurosci Res* 1993; **36**: 663–671.
- Sendtner M, Dittrich F, Hughes RA, Thoenen H. Actions of CNTF and neurotrophins on degenerating motoneurons: preclinical studies and clinical implications. *J Neurol Sci* 1994; **124** (Suppl): 77–83.
- Spector JG, Lee P, Derby A, Friedrich GE, Neises G, Roufa DG. Rabbit facial nerve regeneration in NGF-containing silastic tubes. *Laryngoscope* 1993; **103**: 548–558.
- Li L, Oppenheim RW, Lei M, Houenou LJ. Neurotrophic agents prevent motoneuron death following sciatic nerve section in the neonatal mouse. *J Neurobiol* 1994; **25**: 759–766.
- Barras FM, Pasche P, Bouche N, Aebischer P, Zurn AD. Glial cell line-derived neurotrophic factor released by synthetic guidance channels promotes facial nerve regeneration in the rat. *J Neurosci Res* 2002; **70**: 746–755.
- Kohmura E, Yuguchi T, Yoshimine T, Fujinaka T, Koseki N, Sano A *et al*. BDNF atelocollagen mini-pellet accelerates facial nerve regeneration. *Brain Res* 1999; **849**: 235–238.
- Mohiuddin L, Delcroix JD, Fernyhough P, Tomlinson DR. Focally administered nerve growth factor suppresses molecular regenerative responses of axotomized peripheral afferents in rats. *Neuroscience* 1999; **91**: 265–271.
- Nakamura T, Nawa K, Ichihara A. Partial purification and characterization of hepatocyte growth factor from serum of hepatectomized rats. *Biochem Biophys Res Commun* 1984; **122**: 1450–1459.
- Nakamura T, Nishizawa T, Hagiya M, Seki T, Shimonishi M, Sugimura A *et al*. Molecular cloning and expression of human hepatocyte growth factor. *Nature* 1989; **342**: 440–443.
- Bottaro DP, Rubin JS, Falletto DL, Chan AM, Kmiecik TE, Vande Woude GF *et al*. Identification of the hepatocyte growth factor receptor as the c-met proto-oncogene product. *Science* 1991; **251**: 802–804.
- Hayashi K, Morishita R, Nakagami H, Yoshimura S, Hara A, Matsumoto K *et al*. Gene therapy for preventing neuronal death using hepatocyte growth factor: *in vivo* gene transfer of HGF to subarachnoid space prevents delayed neuronal death in gerbil hippocampal CA1 neurons. *Gene Therapy* 2001; **8**: 1167–1173.
- Caton A, Hacker A, Naeem A, Livet J, Maina F, Bladt F *et al*. The branchial arches and HGF are growth-promoting and chemoattractant for cranial motor axons. *Development* 2000; **127**: 1751–1766.
- Hamanoue M, Takemoto N, Matsumoto K, Nakamura T, Nakajima K, Kohsaka S. Neurotrophic effect of hepatocyte growth factor on central nervous system neurons *in vitro*. *J Neurosci Res* 1996; **43**: 554–564.
- Jin H, Yang R, Li W, Ogasawara AK, Schwall R, Eberhard DA *et al*. Early treatment with hepatocyte growth factor improves cardiac function in experimental heart failure induced by myocardial infarction. *J Pharmacol Exp Ther* 2003; **304**: 654–660.
- Maina F, Klein R. Hepatocyte growth factor, a versatile signal for developing neurons. *Nat Neurosci* 1999; **2**: 213–217.
- Matsumoto K, Nakamura T. Hepatocyte growth factor (HGF) as a tissue organizer for organogenesis and regeneration. *Biochem Biophys Res Commun* 1997; **239**: 639–644.
- Sun W, Funakoshi H, Nakamura T. Overexpression of HGF retards disease progression and prolongs life span in a transgenic mouse model of ALS. *J Neurosci* 2002; **22**: 6537–6548.
- Sun W, Funakoshi H, Nakamura T. Localization and functional role of hepatocyte growth factor (HGF) and its receptor c-met in the rat developing cerebral cortex. *Brain Res Mol Brain Res* 2002; **103**: 36–48.
- Kitamura K, Iwanami A, Nakamura M, Yamane J, Watanabe K, Suzuki Y *et al*. Hepatocyte growth factor promotes endogenous repair and functional recovery after spinal cord injury. *J Neurosci Res* 2007; **85**: 2332–2342.
- Shimamura M, Sato N, Oshima K, Aoki M, Kurinami H, Waguri S *et al*. Novel therapeutic strategy to treat brain ischemia: overexpression of hepatocyte growth factor gene reduced ischemic injury without cerebral edema in rat model. *Circulation* 2004; **109**: 424–431.
- Shimamura M, Sato N, Waguri S, Uchiyama Y, Hayashi T, Iida H *et al*. Gene transfer of hepatocyte growth factor gene improves learning and memory in the chronic stage of cerebral infarction. *Hypertension* 2006; **47**: 742–751.

- 24 Carnicero E, Knipper M, Tan J, Alonso MT, Schimmang T. Herpes simplex virus type 1-mediated transfer of neurotrophin-3 stimulates survival of chicken auditory sensory neurons. *Neurosci Lett* 2002; **321**: 149–152.
- 25 Chattopadhyay M, Goss J, Wolfe D, Goins WC, Huang S, Glorioso JC *et al*. Protective effect of herpes simplex virus-mediated neurotrophin gene transfer in cisplatin neurotoxicity. *Brain* 2004; **127**: 929–939.
- 26 Kato R, Wolfe D, Coyle CH, Huang S, Wechuck JB, Goins WF *et al*. Herpes simplex virus vector-mediated delivery of glial cell line-derived neurotrophic factor rescues erectile dysfunction following cavernous nerve injury. *Gene Therapy* 2007; **14**: 1344–1352.
- 27 Kato R, Wolfe D, Coyle CH, Wechuck JB, Tyagi P, Tsukamoto T *et al*. Herpes simplex virus vector-mediated delivery of neurturin rescues erectile dysfunction of cavernous nerve injury. *Gene Therapy* 2009; **16**: 26–33.
- 28 Walwyn WM, Matsuka Y, Arai D, Bloom DC, Lam H, Tran C *et al*. HSV-1-mediated NGF delivery delays nociceptive deficits in a genetic model of diabetic neuropathy. *Exp Neurol* 2006; **198**: 260–270.
- 29 Coffin RS, MacLean AR, Latchman DS, Brown SM. Gene delivery to the central and peripheral nervous systems of mice using HSV1 ICP34.5 deletion mutant vectors. *Gene Therapy* 1996; **3**: 886–891.
- 30 Coffin RS, Thomas SK, Thomas DP, Latchman DS. The herpes simplex virus 2 kb latency associated transcript (LAT) leader sequence allows efficient expression of downstream proteins which is enhanced in neuronal cells: possible function of LAT ORFs. *J Gen Virol* 1998; **79** (Part 12): 3019–3026.
- 31 Palmer JA, Branston RH, Lilley CE, Robinson MJ, Groutis F, Smith J *et al*. Development and optimization of herpes simplex virus vectors for multiple long-term gene delivery to the peripheral nervous system. *J Virol* 2000; **74**: 5604–5618.
- 32 Lilley CE, Branston RH, Coffin RS. Herpes simplex virus vectors for the nervous system. *Curr Gene Ther* 2001; **1**: 339–358.
- 33 Lindsay RM. Role of neurotrophins and trk receptors in the development and maintenance of sensory neurons: an overview. *Philos Trans R Soc Lond B Biol Sci* 1996; **351**: 365–373.
- 34 Federoff HJ, Geschwind MD, Geller AI, Kessler JA. Expression of nerve growth factor *in vivo* from a defective herpes simplex virus 1 vector prevents effects of axotomy on sympathetic ganglia. *Proc Natl Acad Sci USA* 1992; **89**: 1636–1640.
- 35 Gravel C, Gotz R, Lorrain A, Sendtner M. Adenoviral gene transfer of ciliary neurotrophic factor and brain-derived neurotrophic factor leads to long-term survival of axotomized motor neurons. *Nat Med* 1997; **3**: 765–770.
- 36 Hadlock TA, Heaton J, Cheney M, Mackinnon SE. Functional recovery after facial and sciatic nerve crush injury in the rat. *Arch Facial Plast Surg* 2005; **7**: 17–20.
- 37 Most SP. Facial nerve recovery in bcl2 overexpression mice after crush injury. *Arch Facial Plast Surg* 2004; **6**: 82–87.
- 38 Serpe CJ, Sanders VM, Jones KJ. Kinetics of facial motoneuron loss following facial nerve transection in severe combined immunodeficient mice. *J Neurosci Res* 2000; **62**: 273–278.
- 39 Esslen E. A method of demonstrating and measuring disturbances of central innervation: electrotonomyography. *Electroencephalogr Clin Neurophysiol* 1967; **23**: 387.
- 40 Honda N, Hato N, Takahashi H, Wakisaka H, Kasaki H, Murakami S *et al*. Pathophysiology of facial nerve paralysis induced by herpes simplex virus type 1 infection. *Ann Otol Rhinol Laryngol* 2002; **111**: 616–622.
- 41 Engstrom M, Jonsson L, Grindlund M, Stalberg E. House-Brackmann and Yanagihara grading scores in relation to electroneurographic results in the time course of Bell's palsy. *Acta Otolaryngol* 1998; **118**: 783–789.
- 42 Sugita T, Murakami S, Yanagihara N, Fujiwara Y, Hirata Y, Kurata T. Facial nerve paralysis induced by herpes simplex virus in mice: an animal model of acute and transient facial paralysis. *Ann Otol Rhinol Laryngol* 1995; **104**: 574–581.
- 43 Murakami S, Mizobuchi M, Nakashiro Y, Doi T, Hato N, Yanagihara N. Bell palsy and herpes simplex virus: identification of viral DNA in endoneurial fluid and muscle. *Ann Intern Med* 1996; **124**: 27–30.
- 44 Nishiyama Y. Herpes simplex virus gene products: the accessories reflect her lifestyle well. *Rev Med Virol* 2004; **14**: 33–46.
- 45 Komobuchi H, Hato N, Teraoka M, Wakisaka H, Takahashi H, Gyo K *et al*. Basic fibroblast growth factor combined with biodegradable hydrogel promotes healing of facial nerve after compression injury: an experimental study. *Acta Otolaryngol* 2010; **130**: 173–178.
- 46 Zhao MZ, Nonoguchi N, Ikeda N, Watanabe T, Furutama D, Miyazawa D *et al*. Novel therapeutic strategy for stroke in rats by bone marrow stromal cells and *ex vivo* HGF gene transfer with HSV-1 vector. *J Cereb Blood Flow Metab* 2006; **26**: 1176–1188.
- 47 Liu Y, Michalopoulos GK, Zarnegar R. Molecular cloning and characterization of cDNA encoding mouse hepatocyte growth factor. *Biochim Biophys Acta* 1993; **1216**: 299–303.
- 48 Esaki S, Goshima F, Katsumi S, Watanabe D, Ozaki N, Murakami S *et al*. Apoptosis induction after herpes simplex virus infection differs according to cell type *in vivo*. *Arch Virol* 2010; **155**: 1235–1245.

Repeated treatments with bevacizumab for recurrent radiation necrosis in patients with malignant brain tumors: a report of 2 cases

Motomasa Furuse · Shinji Kawabata ·
Toshihiko Kuroiwa · Shin-Ichi Miyatake

Received: 26 April 2010 / Accepted: 23 July 2010 / Published online: 7 August 2010
© Springer Science+Business Media, LLC. 2010

Abstract Bevacizumab is expected to constitute a new treatment modality for radiation necrosis. In the present cases, we observed a recurrence of radiation necrosis after temporary improvement by bevacizumab treatment. Re-treatment with bevacizumab controlled the necrosis again. A 39-year-old male and a 57-year-old female were diagnosed with glioblastoma and lung cancer metastasis, respectively. The former patient underwent partial resection of the glioblastoma, followed by boron neutron capture therapy (BNCT) and 30 Gy of fractionated X-ray radiotherapy. Eleven months after BNCT, he suffered from left hemiparesis and convulsions with enlargement of a perifocal edema. The latter patient underwent stereotactic radiosurgery twice for the same tumor. Three months after the second radiosurgery, she had an uncontrollable convulsion and right hemiplegia with a massive perifocal edema. Both lesions were suggested to be radiation necroses by positron emission tomography using amino acids as a tracer. Neither patient responded to corticosteroids, anticoagulants, or vitamin E. They underwent treatment with 5 mg/kg bevacizumab biweekly, for a total of 6 cycles. The size of the perifocal edema was clearly reduced in response to the treatments. The neurological status of the patients improved concomitant with therapy. However, the clinical status of both patients was aggravated several months after the bevacizumab was stopped, and the perifocal edemas enlarged again. The patients underwent a second treatment with bevacizumab, and the perifocal edemas again decreased. Although radiation necrosis may

recur several months after bevacizumab treatment, repeated bevacizumab treatments also appear to be effective.

Keywords Bevacizumab · Boron neutron capture therapy · Brain edema · Glioblastoma, metastatic brain tumor · Radiation necrosis

Bevacizumab is a humanized murine monoclonal antibody against the vascular endothelial growth factor (VEGF) ligand that has been approved by the FDA in the U.S. to treat colorectal cancer, non-small cell lung cancer, renal cancer, breast cancer, and glioblastoma multiforme [1–5]. In addition, preliminary studies reported that bevacizumab was effective for treating radiation necrosis in the central nervous system [6, 7]. These studies led to a randomized controlled trial that demonstrated class I evidence of the efficacy of bevacizumab treatment for progressive radiation necrosis [8]. In the present work, we report our use of bevacizumab to treat two patients who showed signs of radiation necrosis after radiotherapy for a metastatic brain tumor and a glioblastoma, respectively. In both cases, rapid improvement was achieved both clinically and neuroradiologically after the initial treatment, but the patients worsened several months after the bevacizumab treatment was stopped, and thus a second round of bevacizumab therapy was used. We report the results of these two cases.

Case 1

A 39-year-old male had a right parietal cystic glioblastoma. Fluoride-labeled boronophenylalanine (BPA)-positron emission tomography (PET) was applied for the residual lesion, and the lesion/normal tissue (L/N) ratio was 3.0

M. Furuse · S. Kawabata · T. Kuroiwa · S.-I. Miyatake (✉)
Department of Neurosurgery, Osaka Medical College, 2-7,
Daigakumachi, Takatsuki, Osaka 569-8686, Japan
e-mail: neu070@poh.osaka-med.ac.jp

(Fig. 1a). This L/N ratio was representative of glioblastoma [9]. An L/N ratio of greater than 2.5 is strongly suggestive of tumor progression in newly-diagnosed or recurrent glioblastomas, while an L/N ratio of less than 2.0 suggests a high possibility of radiation necrosis or pseudoprogression [9, 10]. Tumor-selective particle radiation, boron neutron capture therapy (BNCT) were applied with a minimum tumor dose of 42.3 Gy-Eq and a maximum brain dose of 11.9 Gy-Eq [10, 11]. Here, Gy-Eq (gray-equivalent) corresponds to an X-ray dose that can yield effects equivalent to total BNCT radiation [10]. This treatment was followed by 30 Gy fractionated X-ray treatment, according to our recent protocol [12], and temozolomide as adjuvant chemotherapy. The residual tumor was decreased in size in follow-up magnetic resonance (MR) images.

Eleven months after BNCT, left hemiparesis and convulsions recurred and the MR images showed re-enlargement of the gadolinium-enhanced lesion with perifocal edema (Fig. 2a, b). BPA-PET was re-applied to determine whether the lesion represented a radiation necrosis or local tumor progression. The L/N ratio in this PET was 1.9, which suggested that the lesion was indeed radiation necrosis (Fig. 1b) [9]. Corticosteroids, anticoagulants, and vitamin E were all tried and were not effective.

The patient underwent treatment with bevacizumab of 5 mg/kg biweekly for 6 cycles in total. MR images revealed that the perilesional edema and gadolinium-enhanced lesion were reduced in size, as shown in Fig. 2c,d. The convulsions were controlled with anticonvulsants, and the hemiparesis improved without use of glucocorticoids.

The patient was restarted on treatment with anticoagulants and vitamin E. Six months later, however, his neurological status was aggravated and MR images demonstrated abnormal enhancement and progression of the perifocal edema (Fig. 3a, b). BPA-PET yielded an L/N ratio of 2.1, suggesting the recurrence of radiation necrosis (Fig. 1c). The L/N ratios in Fig. 2b and c were almost the same (1.9 and 2.1), and compatible with radiation necrosis. He was again treated with 5 mg/kg of bevacizumab every other week. After 3 cycles of bevacizumab, MR images again demonstrated a decrease in the perifocal edema and post-gadolinium enhancement (Fig. 3c, d), and the treatment was

Fig. 1 Serial BPA-PET study in Case 1. **a:** BPA-PET just prior to BNCT (L/N ratio: 3.0). **b:** BPA-PET taken at the first aggravation of clinical symptoms and neuroimages (L/N ratio: 1.9). **c:** BPA-PET taken at the 2nd aggravation (L/N ratio: 2.1)

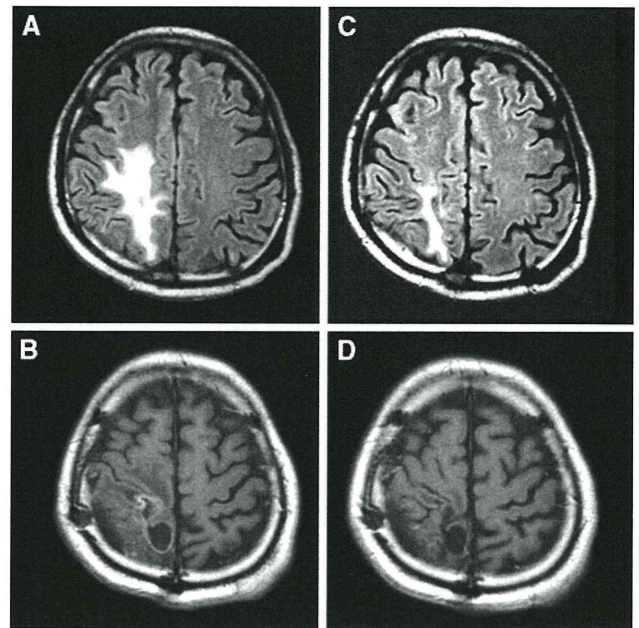
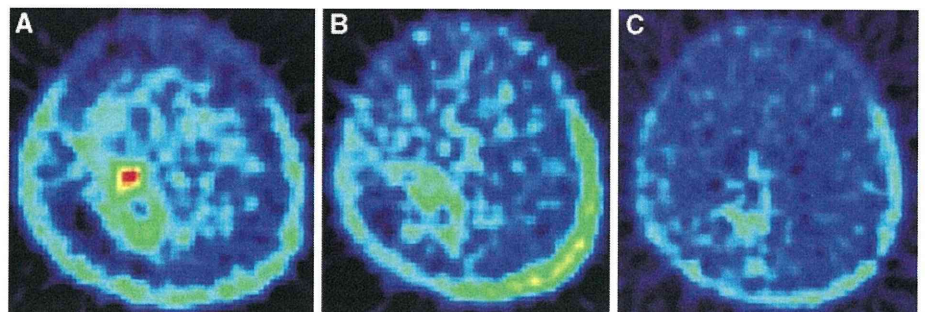


Fig. 2 FLAIR MR images before treatment of bevacizumab (a), and after 6 cycles of bevacizumab 5 mg/kg (c). Postcontrast T1-weighted MR images before treatment with bevacizumab (b), and after 6 cycles of bevacizumab 5 mg/kg (d). *Upper row* an extended hyperintense area obviously reduced after bevacizumab treatment. *Lower row* a postcontrast enhanced lesion indistinct after bevacizumab treatment

stopped. At the time of this writing, the patient has been doing well for more than 4 months without worsening of clinical symptoms.

Case 2

A 57-year-old female experienced a seizure and was diagnosed with a brain metastasis in the left motor strip, which was derived from lung cancer. She underwent repetitive stereotactic radiosurgery (SRS) with a total marginal dose of 49 Gy over a 6-month interval. Three months after the second SRS, her seizures became uncontrollable and right hemiplegia occurred. MR images revealed a progression of perifocal edema and an enhanced lesion (Fig. 4a, b).

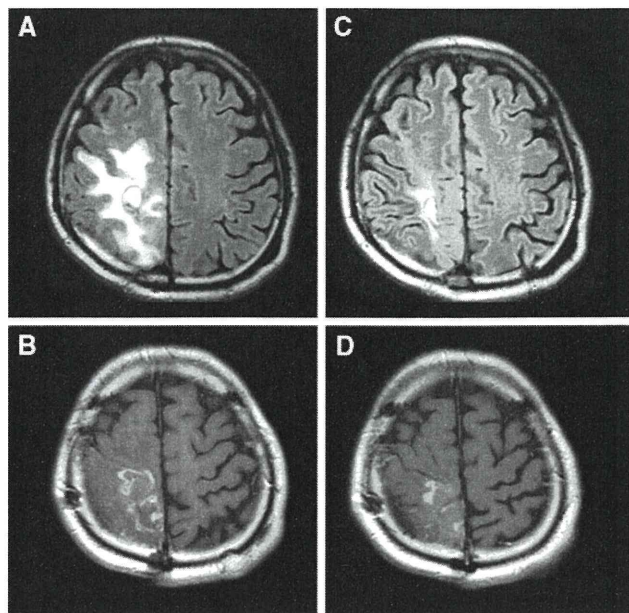
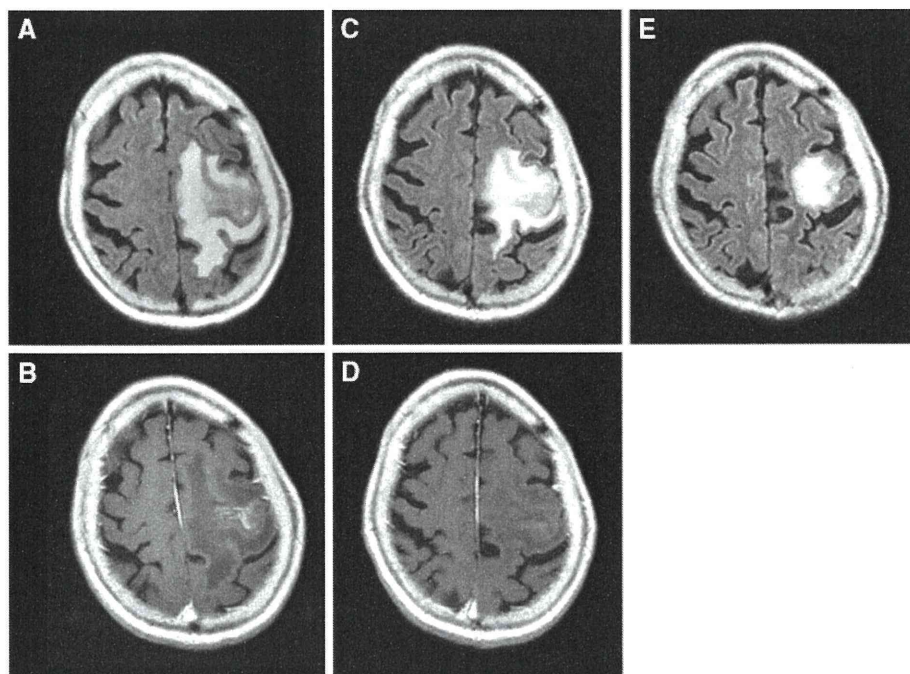


Fig. 3 FLAIR MR images before the second treatment with bevacizumab (a) and after 3 cycles of bevacizumab 5 mg/kg (c). Postcontrast T1-weighted MR images before the second treatment with bevacizumab (b) and after 3 cycles of bevacizumab 5 mg/kg (d). Upper row an enlarged hyperintense area apparently decreased after the second bevacizumab treatment. Lower row postcontrast enhancement became vague after the second bevacizumab treatment

BPA-PET showed a low uptake of BPA, and an L/N ratio of 1.8. Together with the MR findings, these results suggested that the lesion was a radiation necrosis. Her clinical symptoms did not respond to increasing doses of steroids or other medical treatments.

Fig. 4 FLAIR MR images before treatment with bevacizumab (a), 1 week after one dose of bevacizumab 5 mg/kg (c), and after 6 cycles (e). Postcontrast T1-weighted MR images before treatment with bevacizumab (b) and 1 week after one dose of bevacizumab 5 mg/kg (d). Upper row a hyperintense area progressively and dramatically reduced after administration of bevacizumab. Lower row a postcontrast enhancement obscured after bevacizumab treatment



She was treated with 5 mg/kg of bevacizumab every other week. MR images obtained 1 week after one dose showed a dramatic reduction in the hyperintense area on fluid-attenuated inversion recovery (FLAIR) images and attenuation of the abnormal enhanced area on gadolinium-enhanced T1-weighted images (Fig. 4c, d). Subsequent MR images were obtained 1 week after 6 cycles and demonstrated a further decrease in the FLAIR-hyperintense lesion (Fig. 4e). The patient’s hemiparesis consistently improved, and she was able to walk by herself. Her performance status improved from grade 2 to grade 3.

At this time, her treatment was reduced to simply anti-coagulants and vitamin E. Three months later, her hemiparesis was aggravated and computed tomographic imaging revealed an enlarged low-density area (Fig. 5a). She underwent a second bevacizumab treatment. After 2 cycles of bevacizumab, the MR images showed a decrease in perifocal edema (Fig. 5b), but new multiple metastatic lesions. The bevacizumab treatment was therefore discontinued.

Discussion

Recently, new radiation therapies, such as BNCT, SRS, proton beam radiation, and intensity-modulated radiation therapy, have been performed for patients with malignant gliomas. These high-dose radiation therapeutics have been improving patient survival [11–14], but radiation necrosis in the brain has become a more serious problem. Current treatments for radiation necrosis of the brain include the

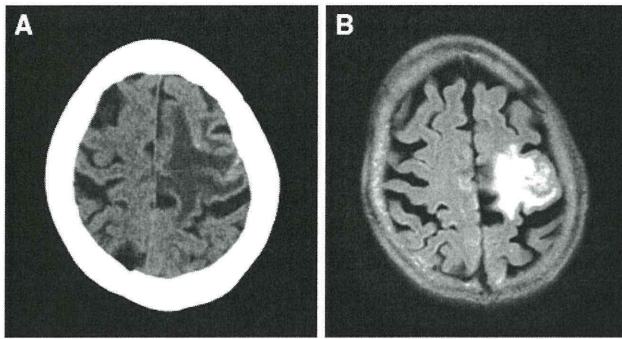


Fig. 5 A computed tomographic image 3 months after the first bevacizumab treatment (a) and a FLAIR MR image after 2 cycles of the second bevacizumab treatment (b). A perilesional edema decreased after the second bevacizumab treatment

use of corticosteroids, anticoagulants, and vitamin E, as well as hyperbaric oxygenation and surgical resection [15–19]. Corticosteroids are often effective in the early phase of radiation injury, but are ineffectual in late radiation injury. Radiation injury includes damage of the vascular endothelial cells, leading to an increase in vascular permeability [20, 21]. Bevacizumab is theoretically effective against radiation injury because VEGF is known as a vascular permeability factor [22]. Gonzalez et al. [6] first reported the effects of bevacizumab on radiation necrosis of brain tumors. They reviewed the cases of 8 patients with recurrent malignant gliomas and radiation necrosis who were treated with bevacizumab, and in some cases with temozolomide or other anticancer agents as well. Radiation necrosis was diagnosed by biopsy in 2 of these patients and by MR images in 6. All 8 patients showed improvement on MR images within 8 weeks of the bevacizumab treatment. Another report by Torcuator et al. [7] also demonstrated the effectiveness of bevacizumab on cerebral radiation necrosis. They confirmed radiation necrosis by biopsy in all 6 patients. Neither of these earlier reports mentioned whether or not radiation necrosis recurred.

In the present case reports, radiation necrosis recurred several months after bevacizumab treatment in both patients. Our patients showed the same initial response to bevacizumab as in the two previous reports. However, in our cases, the bevacizumab treatment did not permanently eradicate the radiation necrosis, and the necrosis recurred. We found bevacizumab effective in treating recurrent radiation necrosis. In the study reported by Levin et al. [8], three patients benefited by retreatment with bevacizumab. In our report, we also found that radiation necrosis can be controlled with bevacizumab treatment as initial treatment as well as in the event of post-bevacizumab recurrence of radiation necrosis.

Our diagnosis of radiation necrosis was based on BPA-PET and serial MR images. Although the findings of

BPA-PET were correlated to histopathological results in our previous study [9], BPA-PET is not a proven radiographic modality. Therefore, our patients were presumed to have radiation necrosis, because the histopathological findings of biopsy or surgical resection are considered definitive for a diagnosis of radiation necrosis. Surgical resection is an important modality if brain edema does not respond to medical treatment and the lesions are resectable. In one of the present cases, because the lesion itself involved the motor strip, a lesionectomy was out of the question. Based on the present findings, bevacizumab can be considered a new treatment modality for both new and recurrent radiation necrosis of the brain, especially for unresectable lesions, as shown here. Its use would influence not only the treatment strategy for radiation necrosis, but also radiotherapeutic dose planning for unresectable tumors.

Conclusion

We used bevacizumab in the treatment of two patients with radiation necrosis of brain tumors. Several months later, however, radiation necrosis recurred in both patients. Repeated therapy with bevacizumab was similarly effective against the recurrent radiation necrosis. Moreover, bevacizumab appears to be an effective treatment for radiation necrosis, especially for lesions located in an eloquent area because radiation necrosis in this area is surgically inaccessible.

Acknowledgments This work was partly supported by a Grant-in-Aid for Scientific Research (B) (19390385 to S.I.M.) from the Japanese Ministry of Education, Science and Culture and in part by the Takeda Science Foundation for Osaka Medical College.

References

1. Hurwitz H, Fehrenbacher L, Novotny W, Cartwright T, Hainsworth J, Heim W, Berlin J, Baron A, Griffing S, Holmgren E, Ferrara N, Fyfe G, Rogers B, Ross R, Kabbinavar F (2004) Bevacizumab plus irinotecan, fluorouracil, and leucovorin for metastatic colorectal cancer. *N Engl J Med* 350:2335–2342
2. Sander A, Gray R, Perry MC, Brahmer J, Schiller JH, Dowlati A, Lilenbaum R, Johnson DH (2006) Paclitaxel-carboplatin alone or with bevacizumab for non-small-cell lung cancer. *N Engl J Med* 355:2542–2550
3. Escudier B, Pluzanska A, Koralewski P, Ravaud A, Bracarda S, Szczlik C, Chevreau C, Filipek M, Melichar B, Bajetta E, Gorbunova V, Bay JO, Bodrogi I, Jagiello-Gruszfeld A, Moore N, AVOREN Trial Investigators (2007) Bevacizumab plus interferon alfa-2a for treatment of metastatic renal cell carcinoma: a randomized, double-blind phase III trial. *Lancet* 370:2103–2111
4. Miller KD, Chap LI, Holmes FA, Cobleigh MA, Marcom PK, Fehrenbacher L, Dickler M, Overmoyer BA, Reimann JD, Sing AP, Langmuir V, Rugo HS (2005) Randomized phase III trial of capecitabine compared with bevacizumab plus capecitabine in